

LARP

11/04/2011
TD-11-021

LARP HQM02 Test Summary

G. Chlachidze, M. Buehler, G. Ambrosio, N. Andreev, E. Barzi, R. Bossert, R. Carcagno, S. Caspi, D. Dietderich, H. Felice, P. Ferracin, A. Ghosh, V.V. Kashikhin, M.J. Kim, M.J. Lamm, F. Lewis, F. Nobrega, I. Novitski, D. Orris, R. Pilipenko, G.L. Sabbi, J. Schmalzle, C. Sylvester, M. Tartaglia, J.C. Tompkins, P. Wanderer, A.V. Zlobin

Content:

1. Introduction	2
2. Structure and Instrumentation	2
3. Quench History	5
4. Ramp Rate Dependence	6
5. Temperature Dependence	8
6. Splice Measurement	8
7. Strain Gauge Data	12
8. Protection Heater Study	25
9. Spike Data Analysis	25
10. Protection heater failure	26
11. Summary	28
References	29
Appendix	30

1. Introduction

HQM02 is a 1.2-m Nb₃Sn coil assembled and tested in a structure designed to provide a quadrupole magnetic field environment (magnetic mirror structure). Coil 13 in the HQ series was fabricated at Lawrence Berkeley National Laboratory (LBNL) as part of the US LHC accelerator research program (LARP) developing large bore (120 mm) interaction region quadrupoles for the LHC luminosity upgrade [1], [2].

The two layer coil in HQM02 uses a 35-strand Rutherford cable with a S2-glass sleeve insulation. 0.8-mm diameter RRP strand of a 54/61 stack cross-section was produced by Oxford Superconductor Technologies, Inc. [3]. Compared to the previously tested coil 12 (HQM01) the azimuthal space for coil expansion during reaction was increased for coil 13. For coil 12, the mid-plane turn was allowed to move below the nominal mid-plane by modifying the shimming in the tooling cavities providing about 3% of additional space per turn. In coil 13, the nominal mid-plane of each layer turn was removed creating around 5% of additional space per turn. This was done to avoid excessive compaction and related azimuthal pressure on the coil during reaction. The above mentioned increase in the azimuthal space was provided in addition to the nominal value of 2% of space per turn used in all previous HQ coils. Another difference in design of coil 13 was an axial gap of 2.2 mm introduced between the 2 pole pieces accounting for 1 mm/m of winding relaxation and 2 mm/m of conductor shrinkage after reaction.

The HQM02 magnet was tested in the Vertical Magnet Test Facility (VMTF) at Fermilab [4]. The test plan included quench training and ramp rate dependence studies at 4.6 K and 2.2 K. The dewar header assembly used for this test does not allow cool-down to a superfluid helium temperature.

The magnet was installed in the VMTF dewar and was electrically checked by September 9th, 2011. The VMTF dewar was filled with liquid helium by September 12th. The test was started on September 12th and was interrupted after few quenches to investigate protection heater failure. More details on protection heater failure will be presented in Sections 3 and 10. The test was completed on October 21st and the magnet was removed from the VMTF dewar on November 9th.

2. Structure and Instrumentation

A quadrupole magnetic mirror structure was developed at Fermilab to provide an efficient and fast way to test and optimize Nb₃Sn quadrupole coils. This structure tests individual coils under operating conditions similar to that of a real magnet, thus reducing the turnaround time of coil fabrication and evaluation, as well as material and labor costs. Previously, TQ quadrupole coils were successfully tested in a mirror structure to study the effect of pre-stress on Nb₃Sn coil performance [5].

HQM02 is the second HQ coil tested in a mirror structure (see Fig. 1, left). This structure is similar to the structure used for TQ coils [5], using the iron yoke, iron mirror blocks and a bolt-on skin. Preload is applied by a series of shims placed radially and azimuthally on the coil, and to the upper surface of the side “ears” on the mirror block (-130 MPa were applied at room temperature).

The magnetic flux distribution in the HQM02 cross section is shown in Fig. 1, right.

HQ coil 13 is equipped with 4 protection heaters, 2 in each coil layer (see Fig. 2). Protection heaters were made of stainless steel with 6.0-6.5 Ohm resistance at room temperature. All heater signals were brought to the distribution box at VMTF where the final connections were made to the heater firing units (HFU).

The HQM02 voltage tap system covers both inner and outer coil layers, pole turn, multi-turn and splice sections (see Fig. 3). There are 10 voltage taps in the inner layer and 10 voltage taps in the outer layer.

21 strain gauges (SG) were installed on the shell, coil and bullets to monitor mechanical strain and to calculate coil stresses during magnet construction and testing. There are only 2 SG on the titanium pole pieces which consist of active and temperature-compensating gauges connected into a full-bridge circuit. All other gauges are single gauges installed on the shell and the bullets. Temperature-compensating gauges were mounted on upper and lower half-skis and on lead-end and return-end bullets.

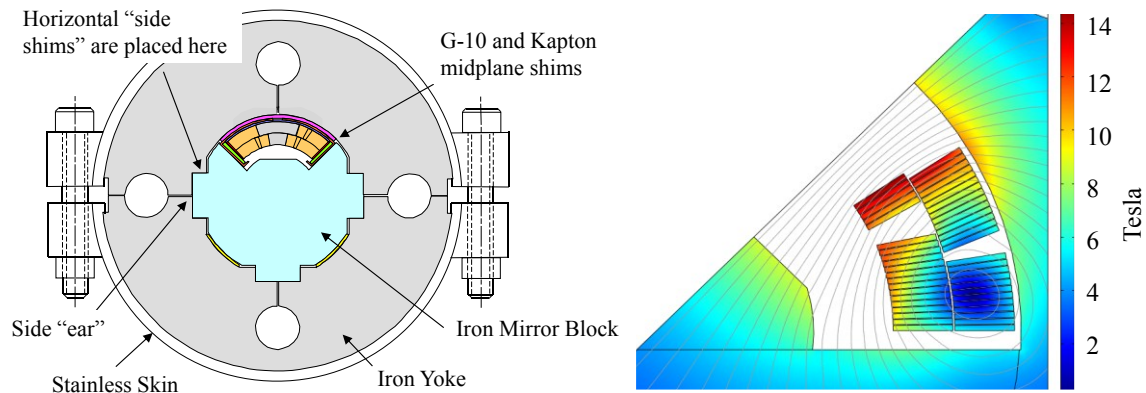


Fig. 1: HQ mirror structure (left) and HQ mirror cross section with flux distribution at 20 kA (right). Peak field at inner pole is 14.9 T.

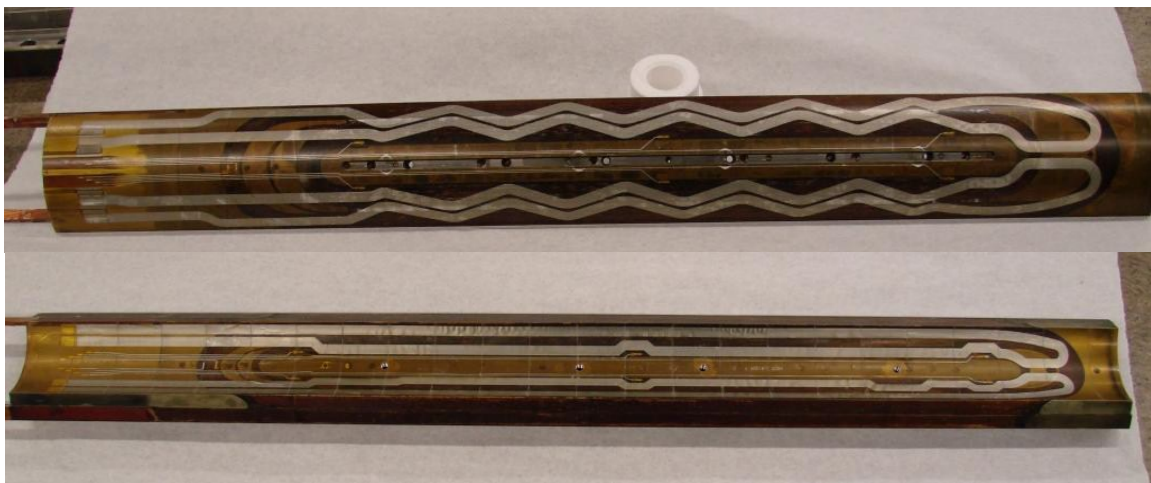


Fig. 2: Outer layer (top) and inner layer (bottom) heaters in HQ coil 13

In addition to the standard set of dewar temperature sensors, 2 additional resistive temperature devices (RTD) were mounted at the top and the bottom of the outer magnet skin (*Cernox cx43235* and *cx43233* sensors respectively).

Since the mirror structure does not have room for a magnetic warm bore, flat printed circuit board (PCB) quench antennas were used to localize quenches. 4 cm boards were distributed evenly with 30 cm spacing (see Fig. 4).

Both VME- and FPGA-based quench detection systems were used in this test. Current-dependent thresholds were used for half-coil signals in both systems. The 1st (2nd) half-coil signal is formed by the inner (outer) coil.

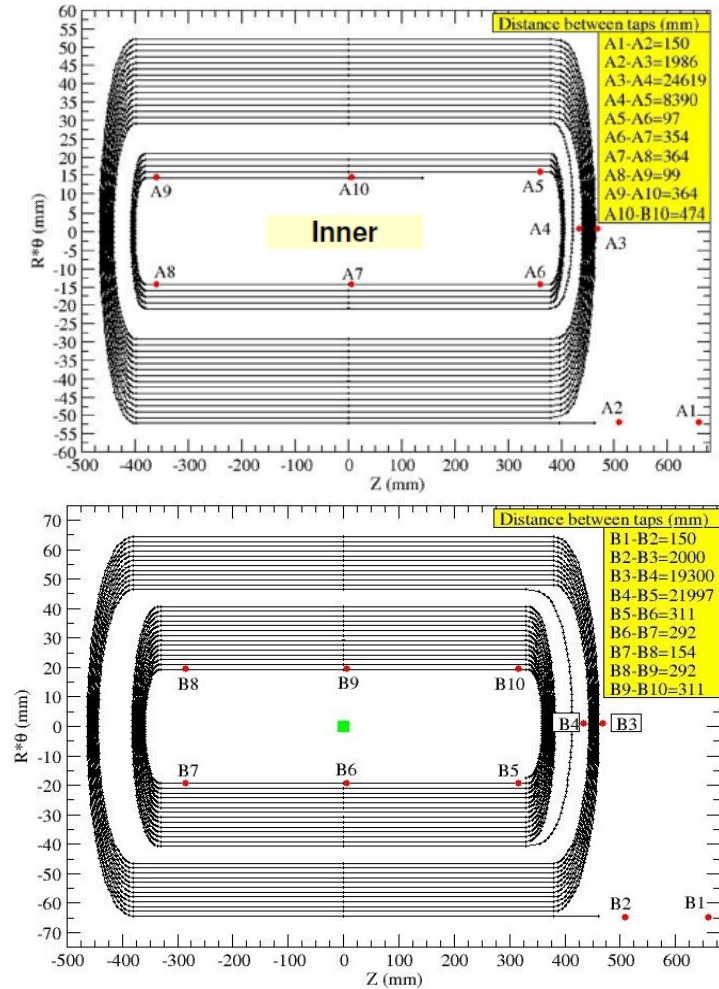


Fig. 3: HQM02 voltage tap locations for the inner (top) and outer (bottom) layers.

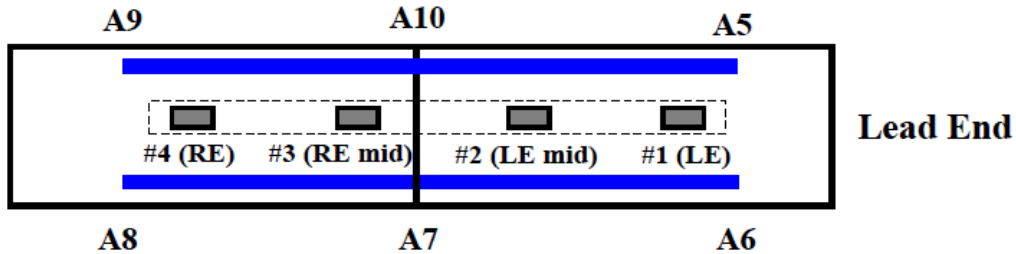


Fig. 4: Quench antenna location in HQM02.

3. Quench History

The first two quenches at 20 A/s initiated in the pole turn segment of the outer coil layer (**b8_b7** in Fig. 3) with quench currents of 13.6 kA and 14 kA, respectively. The next quench developed in the ramp segment (**a10_b10** in Fig. 3) with a significantly higher quench current of 15.7 kA. This quench also resulted in an electrical short between both outer layer protection heaters and the magnet coil. The test was briefly interrupted to address possible safety concerns. Details of this study and post-test analysis of the heater failure are presented in Section 10. Subsequent tests were done without the outer layer protection heaters. Inner layer protection heaters were still functional.

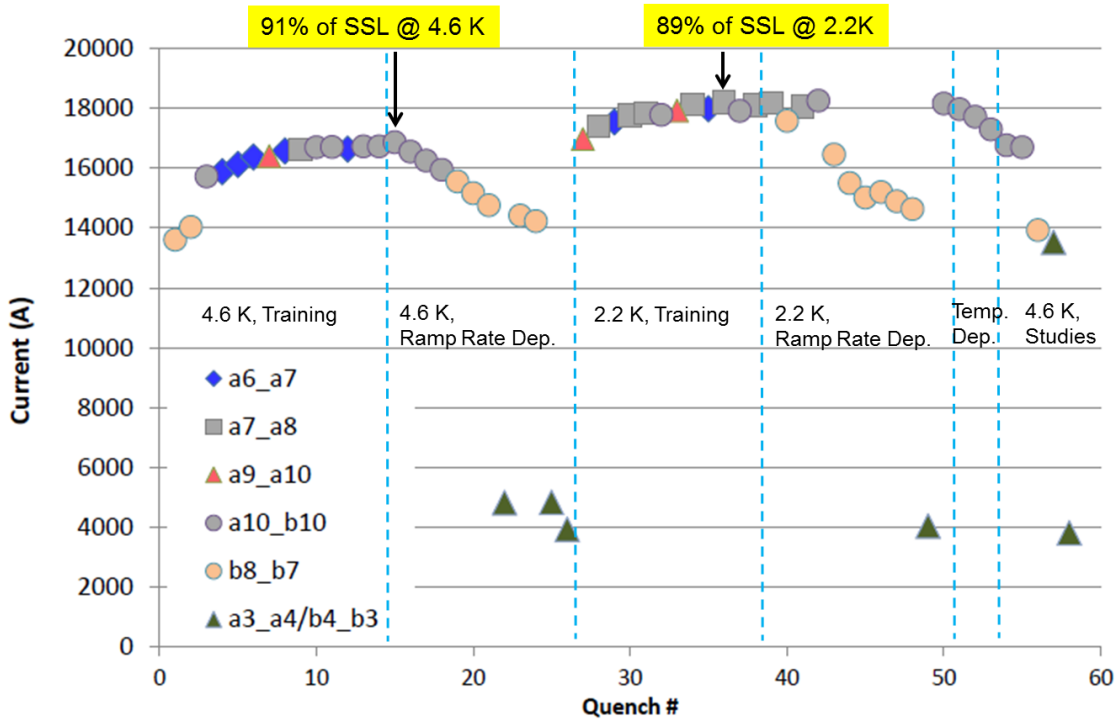


Fig. 5: HQM02 quench history with quench locations.

Following the 3rd training quench, HQM02 exhibited normal training behavior with quenches in high-field region of the inner layer pole turn block (segments **a6_a7**, **a7_a8**, **a9_a10**). After 14 training quenches, a quench current plateau of approximately 16.7 kA was reached, and quenches were mostly developing in the ramp segment (**a10_b10**).

After training, ramp rate dependence studies were done (see Section 4). The first quench at a temperature of 4.6 K and a ramp rate of 5 A/s reached 91% of the Short Sample Limit (SSL).

Subsequently, the dewar temperature was lowered to 2.2 K, followed by a series of training quenches at a ramp rate of 20 A/s. During training at 2.2 K, quenches mostly initiated in high-field regions of the inner layer pole turn block (segments **a6_a7**, **a7_a8**, **a9_a10**). Two last plateau quenches were located in the ramp segment **a10_b10**. During this part of the test, a SSL of 89% was reached.

After training at 2.2 K, ramp rate dependence studies were done (see Section 4), followed by temperature dependence studies (see Section 5).

At the end of testing, various studies were performed at a dewar temperature of 4.6 K. To re-establish a quench plateau for a ramp rate of 20 A/s and a temperature of 4.6 K, two verification quenches were initialized, resulting in quench currents of 16.7 kA (**a10_b10**) as expected. The following two quenches were preceded by conditioning ramps, i.e., ramping to 10 kA at a rate of 150 A/s, then ramping back to 0 A, and finally ramping to quench at 400 A/s and 450 A/s. This resulted in quench currents of 13.9 kA (**b8_b7**) and 13.5 kA (**a3_a4**, **b3_b4**), respectively. Repeating the quench at 450 A/s without performing a conditioning ramp resulted in a quench current of 3.8 kA (**a3_a4**, **b3_b4**).

A final sequence of ramp-down tests was performed, ramping to 14 kA at a rate of 150 A/s, followed by ramp-downs at varying ramp rates. No quenches were observed when varying the ramp-down rate from 50 A/s to 400 A/s in steps of 50 A/s.

The Residual Resistivity Ratio (RRR) was measured during magnet warm up. On average, RRR values varied from 220 to 285 (Fig. 6).

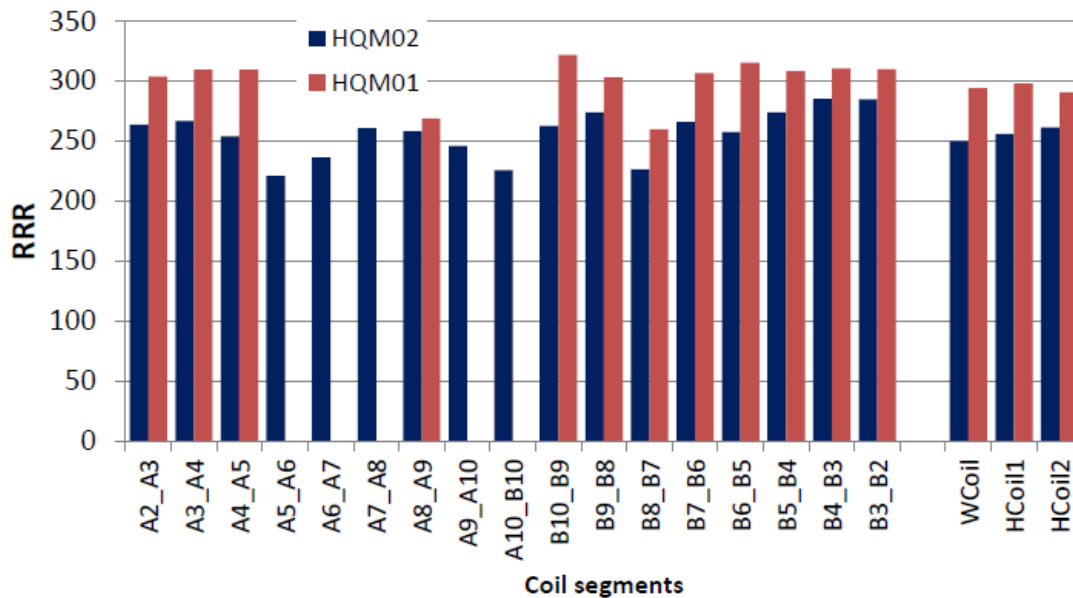


Fig. 6: RRR measurements for HQM02 (blue) and HQM01 (red) for comparison.

Quench performance of HQM01 and HQM02 magnets are compared in Fig. 7. Two 120 mm bore quadrupole coils of the HQ design have been tested in a quadrupole mirror structure under identical pre-load conditions.

4. Ramp Rate Dependence

A history of ramp rate dependence is presented in Fig. 8. At 4.6 K, quenches in the range of 5 A/s to 150 A/s occurred in the ramp segment (**a10_b10**) while at higher ramp rates (200 A/s to 375 A/s) quenches occurred in the **b7_b8** outer layer pole turn segment. Above 375 A/s the quench current dropped sharply from 14.2 kA to <5 kA. In this range quenches were located in the multi-turn mid-plane segments of both inner and outer layers (**a3_a4**, **b3_b4**).

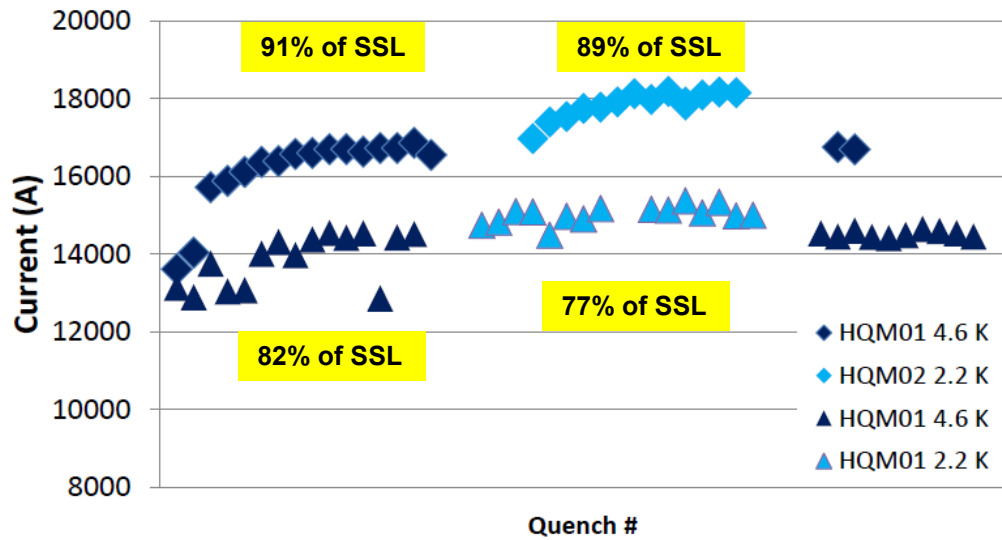


Fig. 7: HQM01 and HQM02 quench training at 4.6 K and 2.2 K

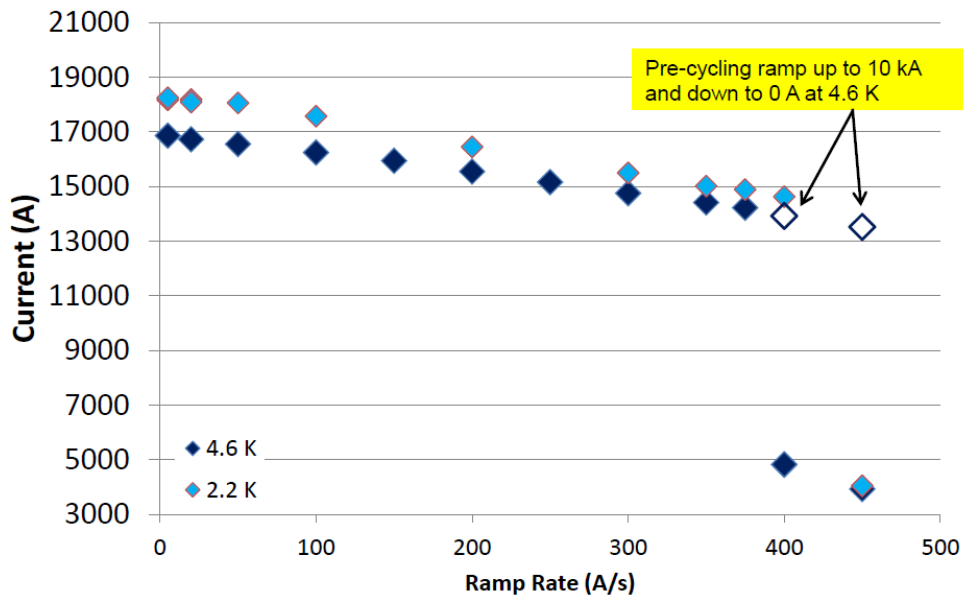


Fig. 8: Quench current as a function of ramp rate for 2.2 K (light blue), 4.6 K (dark blue), and 4.6 K with conditioning ramps (white).

It was empirically found that conditioning ramps up to 10 kA and then down to 0 A helped to avoid the sharp drop of quench current at ramp rates of 400 A/s and 450 A/s (see Fig. 8). Repeating the quench at 450 A/s without performing a conditioning ramp resulted again in a low quench current of 3.8 kA.

At 2.2 K, quench locations at low ramp rates (5 A/s to 50 A/s) were in the inner layer pole turn (**a7_a8**) and the ramp segment (**a10_b10**), while at higher ramp rates (100 A/s to 400 A/s) quenches occurred in the **b7_b8** outer layer pole turn segment. At 450 A/s the

quench current also dropped sharply from 14.6 kA to 4 kA, and the quench location moved to the multi-turn mid-plane segment **a3_a4**.

5. Temperature Dependence

A history of temperature dependence is presented in Fig. 9. Quench behavior as a function of temperature showed a normal trend. Quench currents decreased from 18.1 kA at 2.2 K to 16.7 kA at 4.6 K. All quenches occurred in the ramp segment (**a10_b10**).

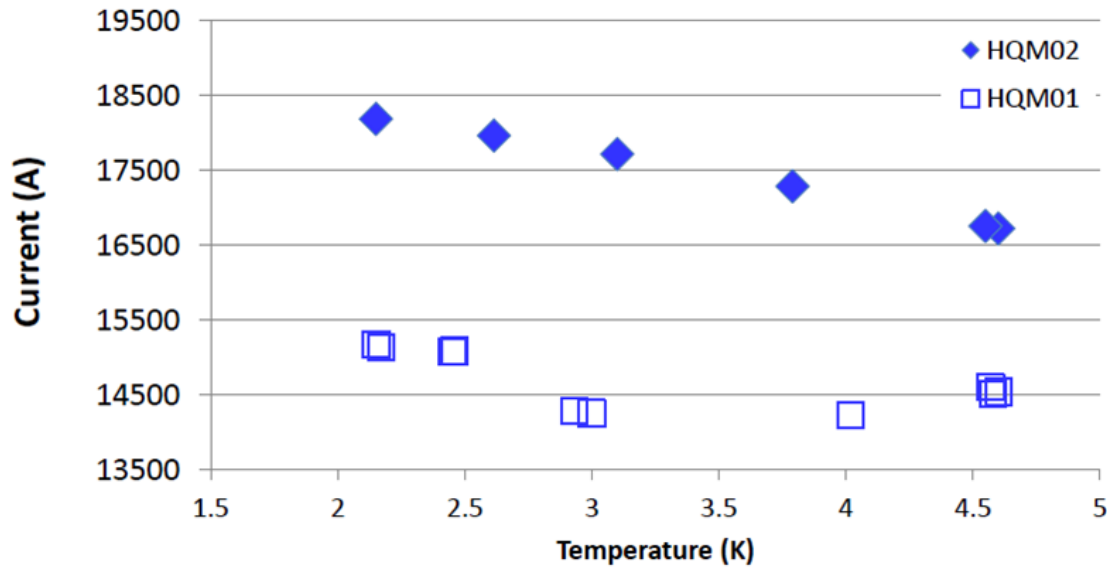


Fig. 9: Quench currents as a function of temperature for HQM02 (solid diamonds) and HQM01 (open squares) for comparison.

6. Splice Measurements

Inner layer Nb₃Sn-NbTi splice resistances (**a1_a2** in Fig. 3) were measured at 4.6 K with typical values in the range of a few nΩs. The general method for our measurement is based on the assumption that the splice resistance is constant, and does not change while an electrical current passes through a splice segment. By ramping a current (I) through the magnet coil and measuring the voltage drop (V) on the splice segment, the resistance of the splice can be measured by evaluating slope of the V vs. I dependence. For a current of 10 kA the expected voltage drop is ~10μV, requiring a precise Digital Multi Meter (DMM), e.g. the *HP-3458 of Agilent Technologies*, with a range of 100 mV and a resolution of 10 nV [6].

Since the measured signals are very small, extra attention was paid to the wiring and noise mitigation. Fig. 10 shows signals from two splices of HQM02 at a current of 8 kA in the magnet coil. The measurement was performed using a FLUKE 199C scope meter. Cables coming from the voltage taps were directly connected to oscilloscope inputs (the external shield of the cable was connected to the cryostat case). ±40mV signals at 720 Hz

(large spikes in Fig. 10) and $\pm 15\text{mV}$ signals at 60 Hz were observed. The 720 Hz noise was attributed to the PEI current source while the 60 Hz noise was attributed to the Active Ground Fault power supply. Such big levels of noise in the DMM input make it difficult to measure μV signals.

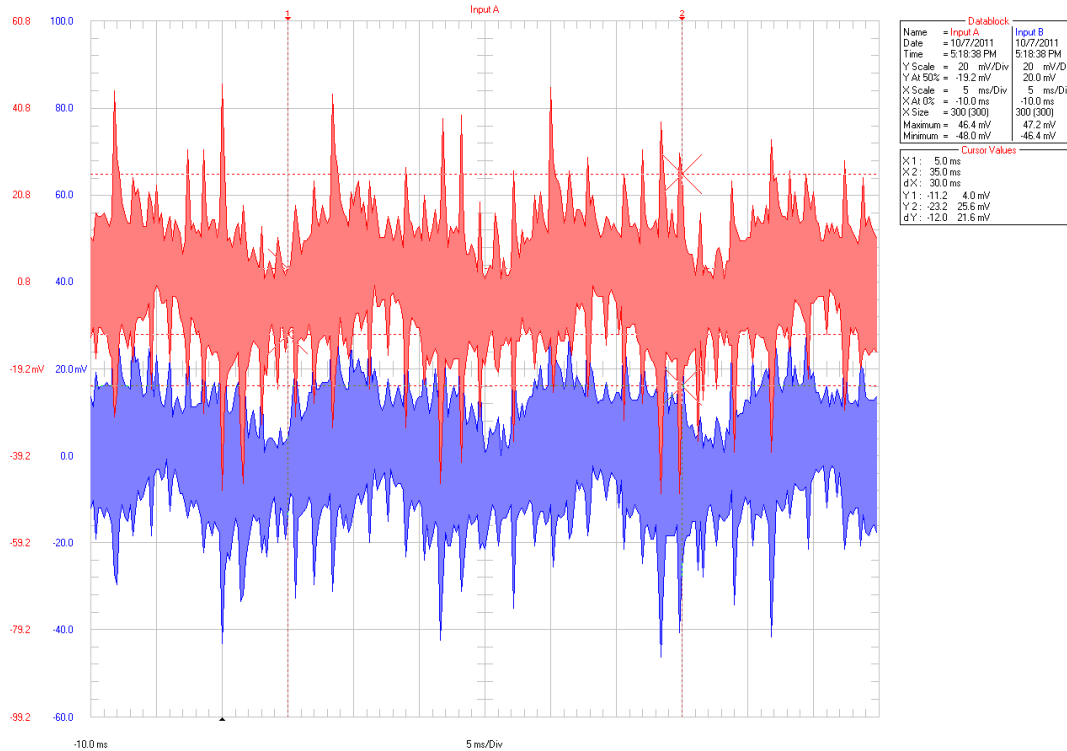


Fig. 10: HQM02 splice signals at 8 kA.

For a splice resistance measurement only the DC component is important. Therefore, a filter can be added at the input of the DMM. If the filter has a low cutting frequency, it decreases the level of unwanted noise enough to observe a changing voltage drop over the splice segment.

For our measurement a simple RC filter was added at the DMM inputs. Externally added filter elements consisted of two 10 k Ω resistors and a 10 μF capacitor (Fig. 11).

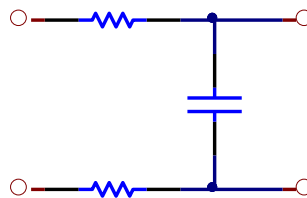


Fig. 11: RC filter used for splice measurements.

With a total resistance of 20 k Ω and a capacitance of 10 μF , the resulting filter cutting frequency is:

$$f = \frac{1}{2\pi RC} = \frac{1}{2\pi \cdot 20k\Omega \cdot 10\mu F} \cong 796\text{mHz}$$

Such a filter should decrease 720 Hz noise ($\pm 40\text{mV}$) ~ 900 times (Fig. 12), so that the level of 720 Hz noise at the DMM inputs is no larger than $\pm 44\mu\text{V}$.

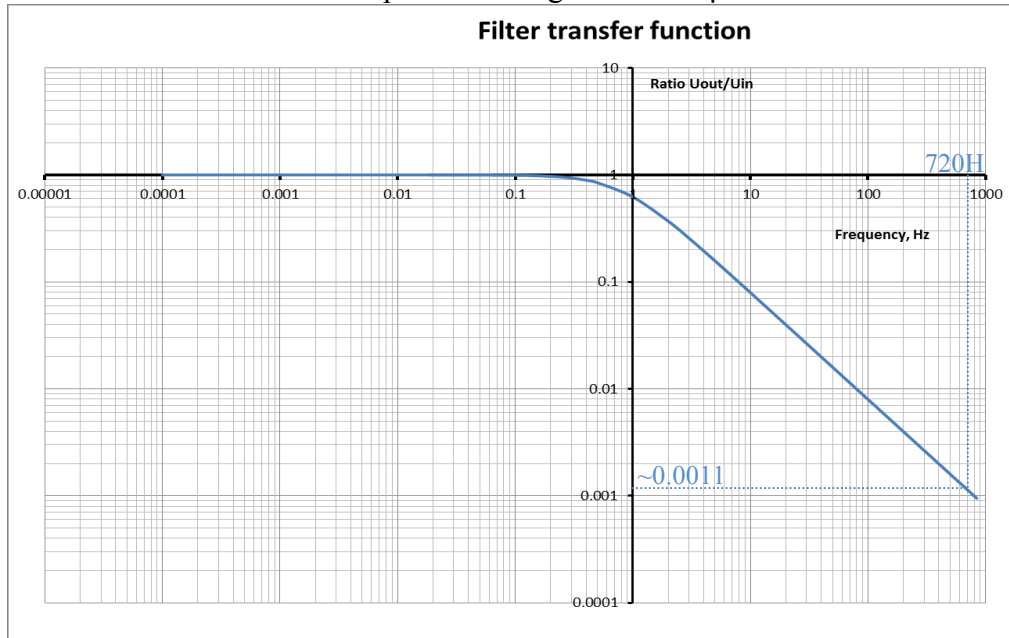


Fig. 12: RC filter transfer function.

60 Hz noise ($\pm 15\text{ mV}$) will be decreased ~ 75 times and should be at the level of $200\ \mu\text{V}$. This noise was significantly reduced when turning off the Active Ground Fault power supply, and further reduced by using a double shielded twisted pair cable as well as DMM guarding. The final scheme for cable and filter connections is shown in Fig. 13.

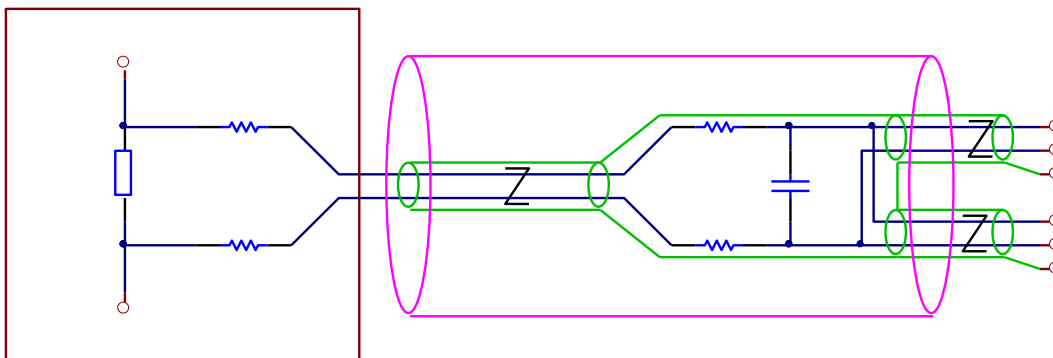


Fig. 13: RC filter and cable connections for splice resistance measurement.

Internal (green) and external (pink) shield connections are shown. The internal shield was connected to the DMM guard and the external shield was connected to the cryostat case.

There is no connection between internal and external shields. The filter was assembled so that both shields completely covered all cables and elements of the filter (Fig. 14).

Internal shield covering filter elements **External shield connected to metal box case through metal connector shells**

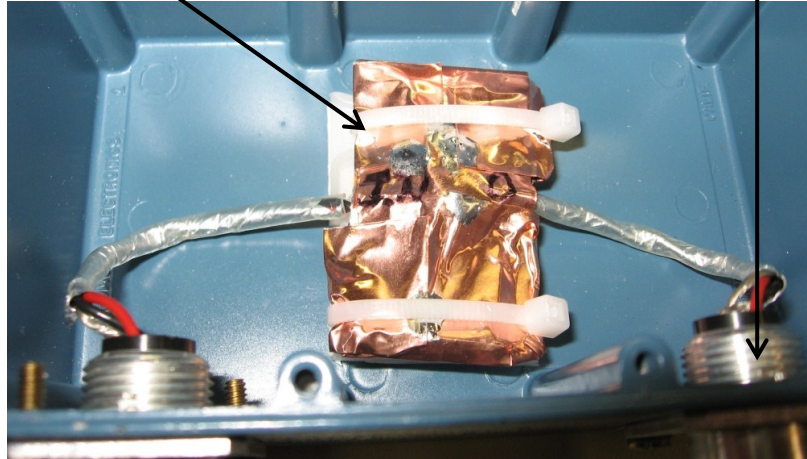


Fig. 14: Shielding for splice resistance measurement.

Fig. 13 shows a differential connection to the DMM, i.e., the output of the filter is split between two DMMs. During testing, a single DMM scheme was used. In comparison with the differential scheme, the single scheme yielded similar results for the splice resistance measurement, although noise levels were larger.

The differential scheme eliminates a possible asymmetry between HI and LO DMM terminals. Additionally, averaging the measured values from two DMMs further decreases noise level (Fig. 15). Noise levels in measured signals were reduced to 500 nV peak-to-peak after filtering and shielding cables.

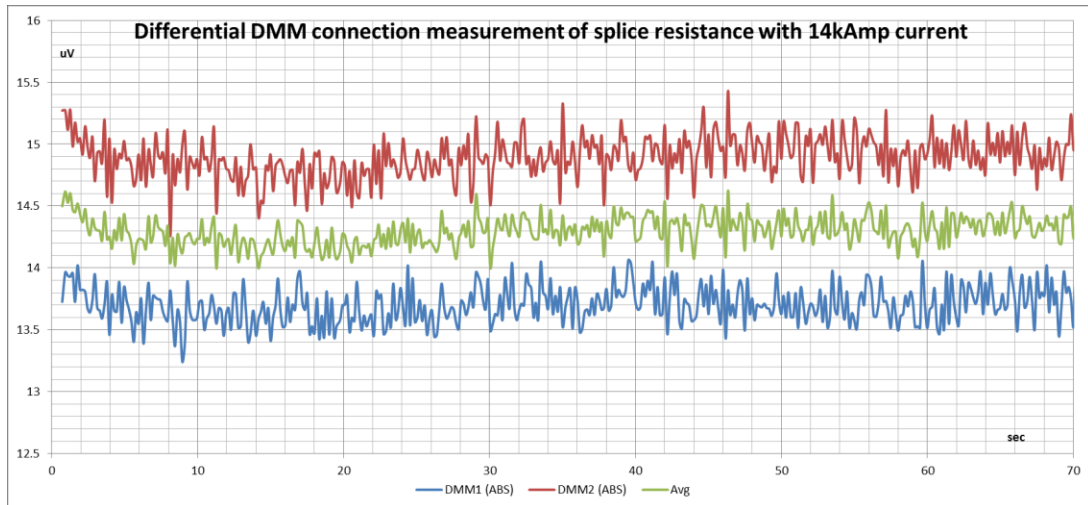


Fig. 15: Differential measurement of splice resistance with averaging HI and LO (green).

Two HP-3458 DMMs controlled through a GPIB interface by a PXI controller were used for this measurement.

For DMM control, a LabView program was designed. The LabView program allowed single measurements in synch with the power line signal. It also ensured that both DMMs were performing the measurement simultaneously.

For the final measurement, the magnet current was varied from 2 kA to 14 kA. Measurement data and a linear fit to data are shown in Fig. 16. The a1_a2 splice resistance was found to be 0.25 nΩ.

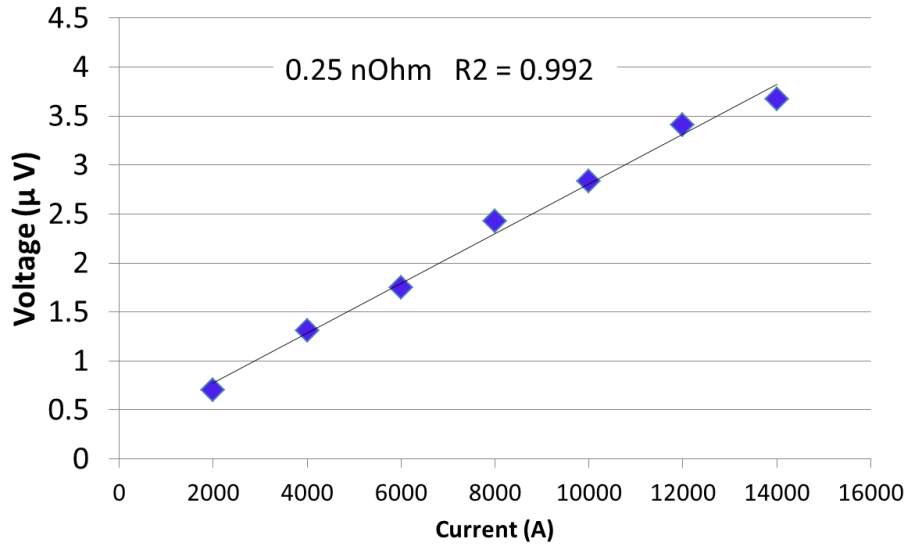


Fig. 16: HQM02 splice resistance measurements.

7. Strain Gauge Data

The mechanical behavior of HQM02 during cool-down, test, and warm-up was monitored with strain gauges mounted on the support structure components and the coil. The coil was instrumented with full bridge azimuthal and axial gauges located in the middle of the titanium pole piece of the inner coil layer. A total of eight bullet-type gauges were used to measure the end forces, two per “bullet” and 2 “bullets” per end. Readings of 2 gauges on the same bullet were averaged to eliminate strains due to bending.

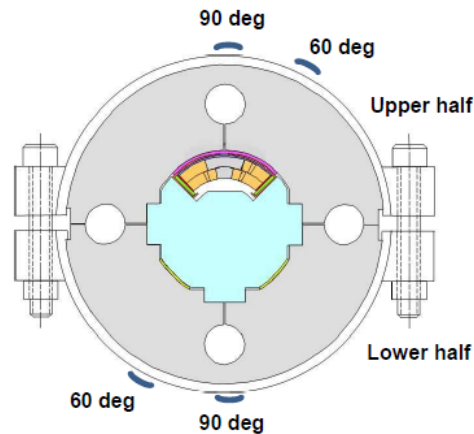


Fig. 17: Skin strain gauges.

The skin was instrumented with a standard set of strain gauges at 90 and 60 degrees in an azimuthal plane both on the upper and lower half-skins (Fig. 17).

One compensating gauge was placed at each end of the magnet and one on the upper half-skin.

In total, 21 strain gauges were installed in HQM02. The following sub-sections illustrate the mechanical behavior of HQM02 during cool-down (7.1), excitation (7.2) and warm-up (7.3).

7.1 Cool-down

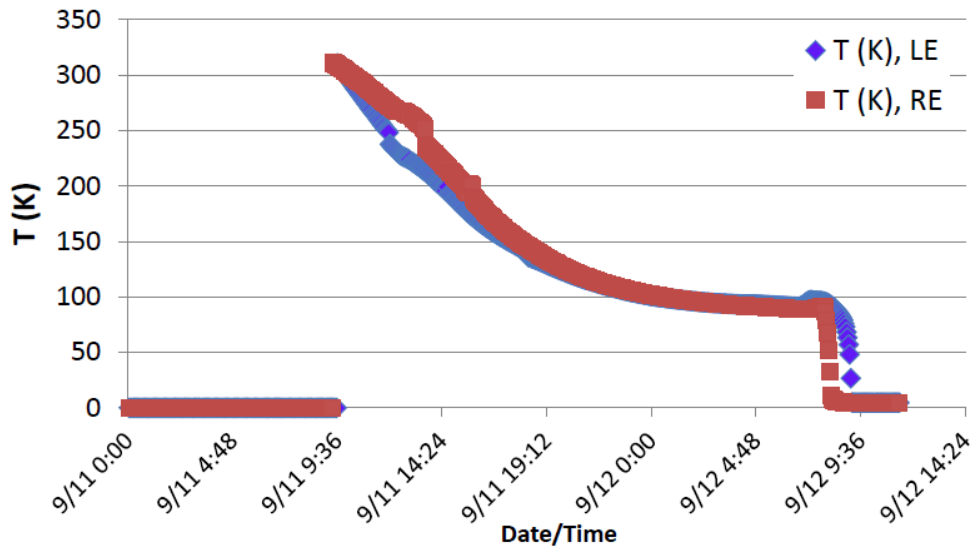


Fig. 18: Magnet skin temperature at LE and RE measured during cool-down vs. time.

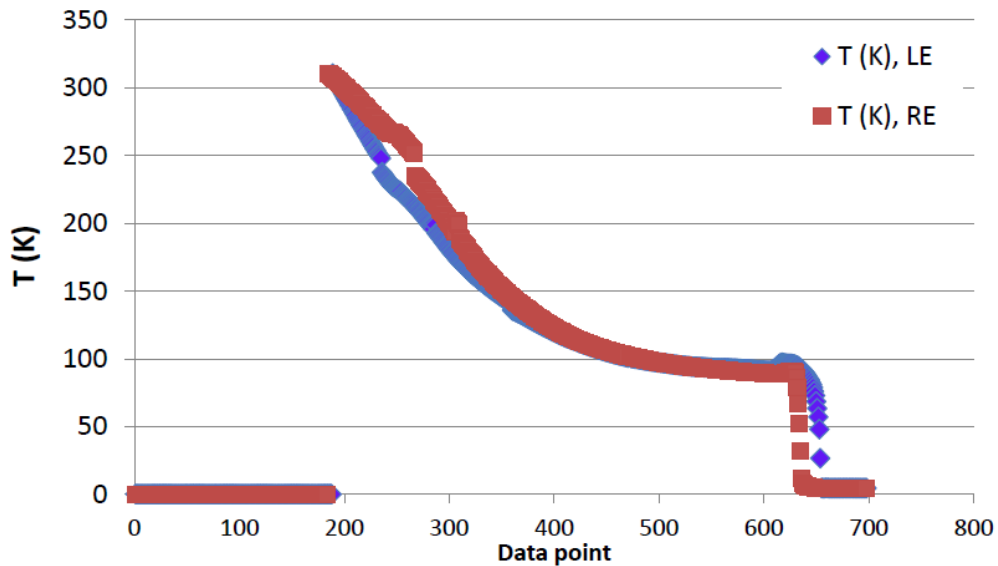


Fig. 19: Magnet skin temperature at LE and RE measured during cool-down vs. data point

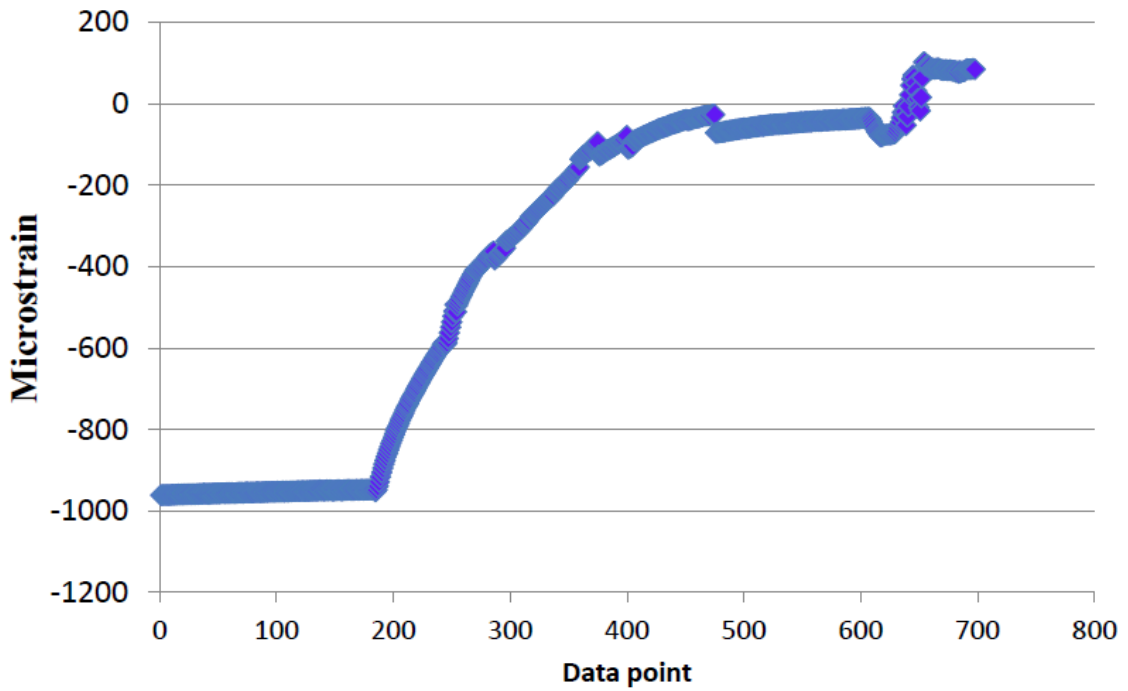


Fig. 20: Azimuthal microstrain in the coil pole measured during cool-down.

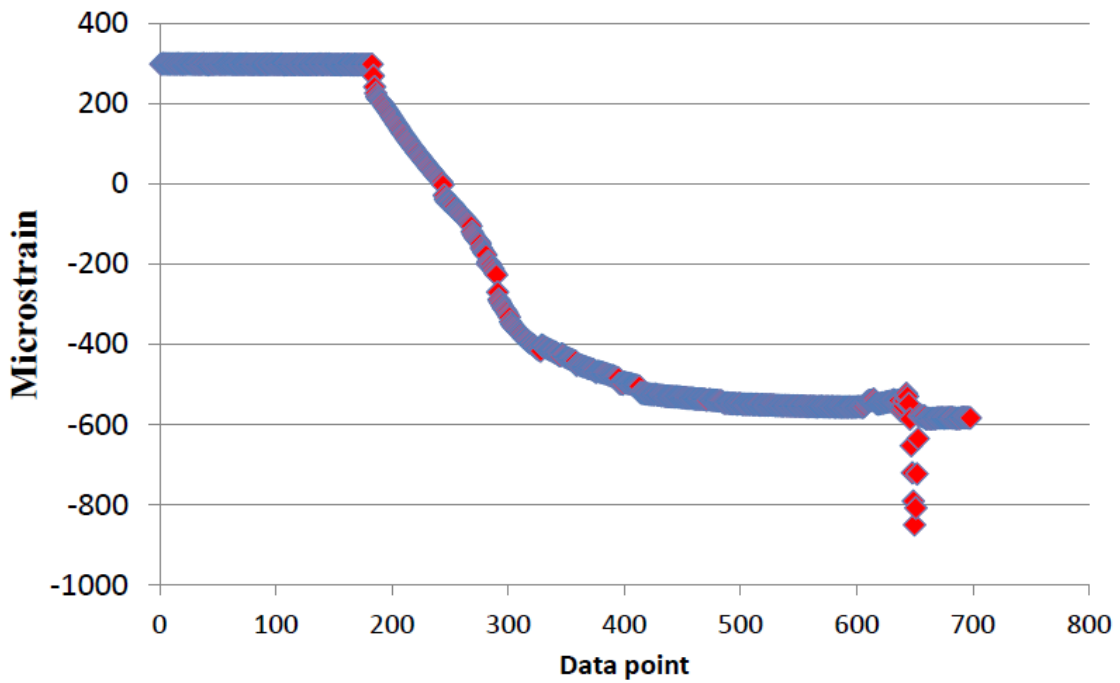


Fig. 21: Axial microstrain in the coil pole measured during cool-down.

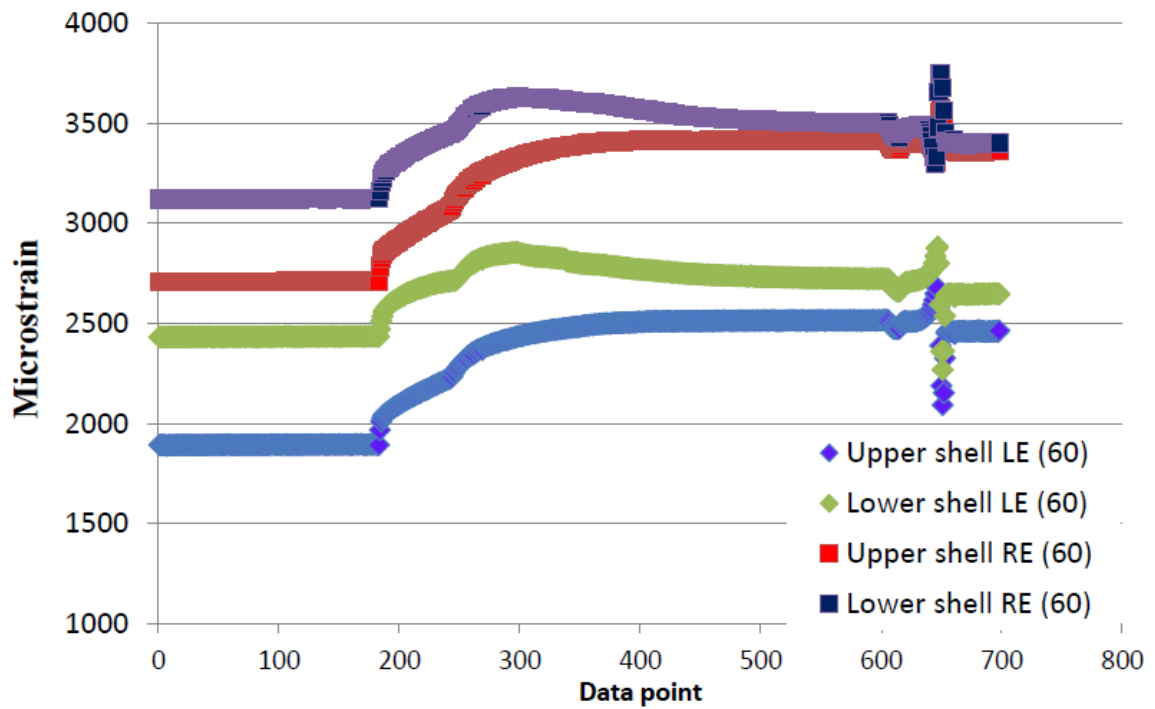


Fig. 22: Skin gauges at 60° during cool-down.

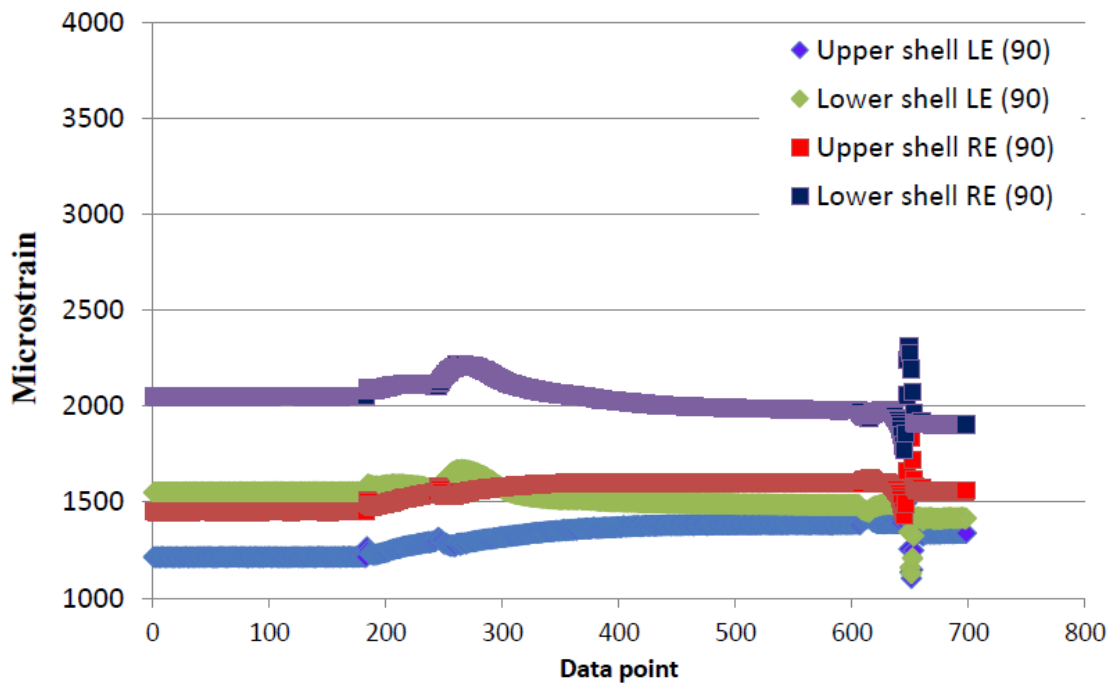


Fig. 23: Skin gauges at 90° during cool-down.

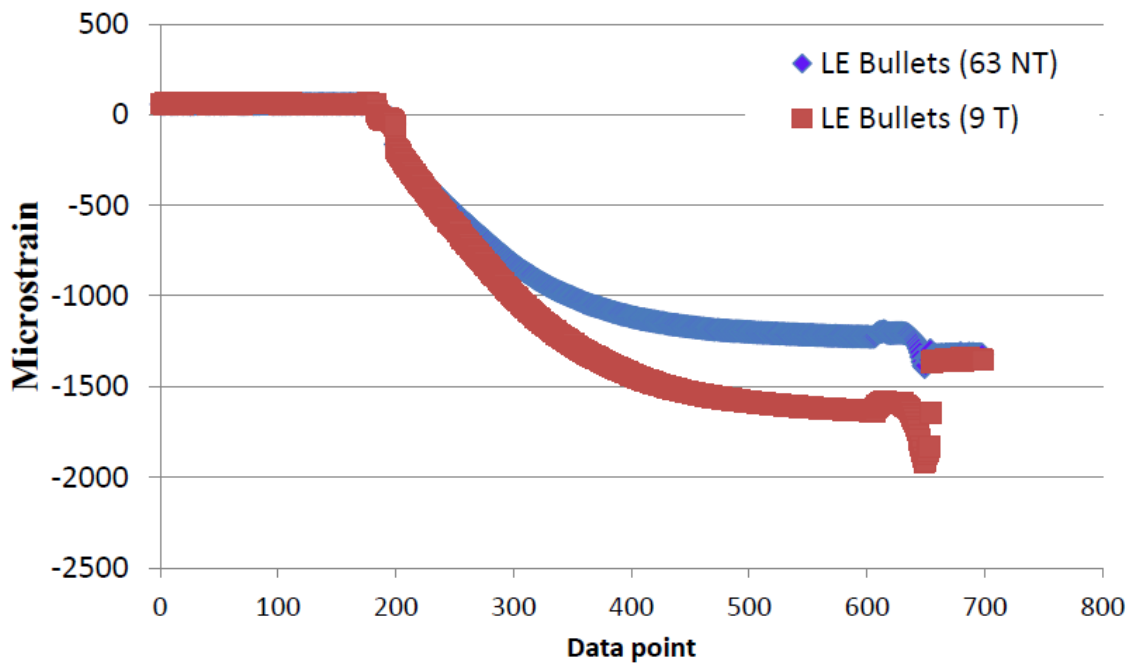


Fig. 24: LE bullet gauges during cool-down.

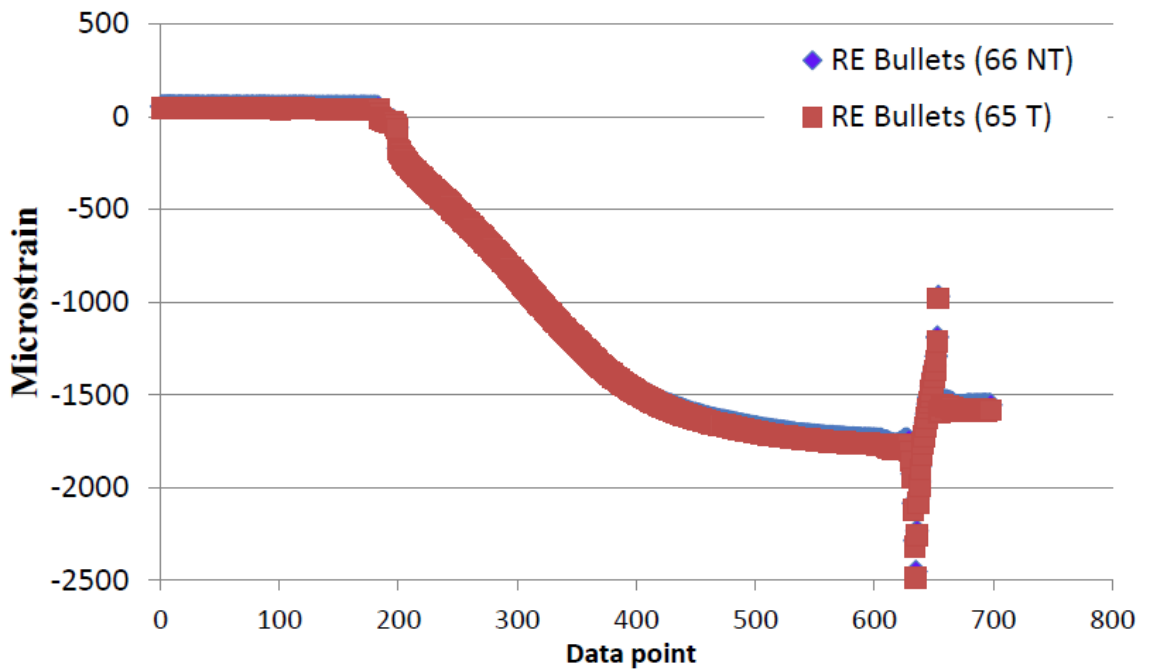


Fig. 25: RE bullet gauges during cool-down.

7.2 Excitation

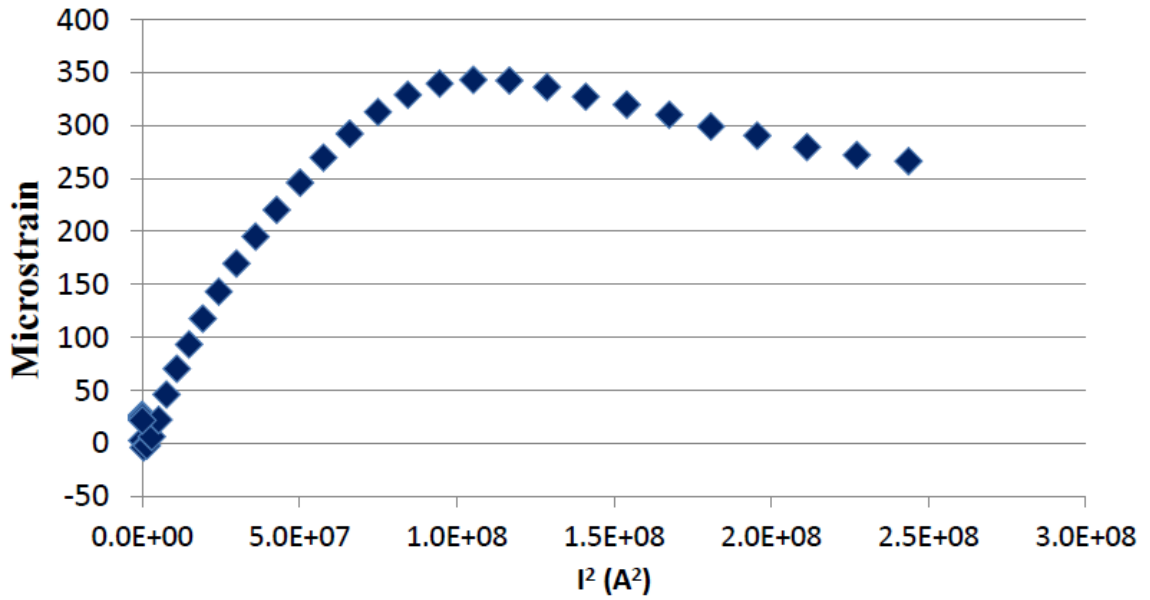


Fig. 26: Azimuthal microstrain in the coil pole vs. I^2 (A^2) for quench 46 (14.6 kA).

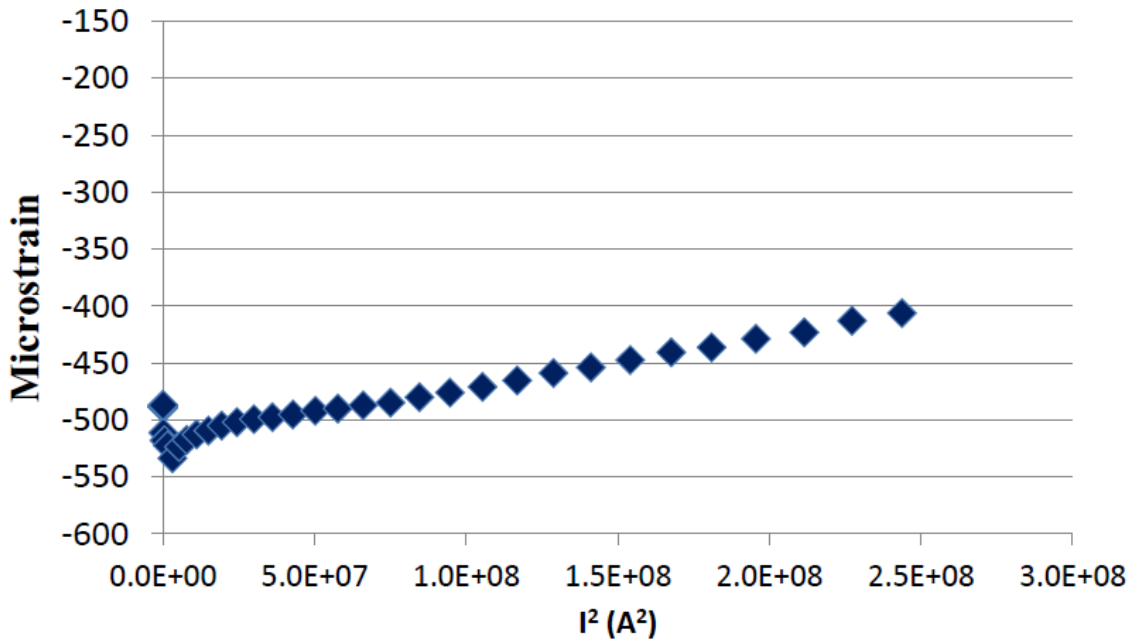


Fig. 27: Axial microstrain in the coil pole vs. I^2 (A^2) for quench 46 (14.6 kA).

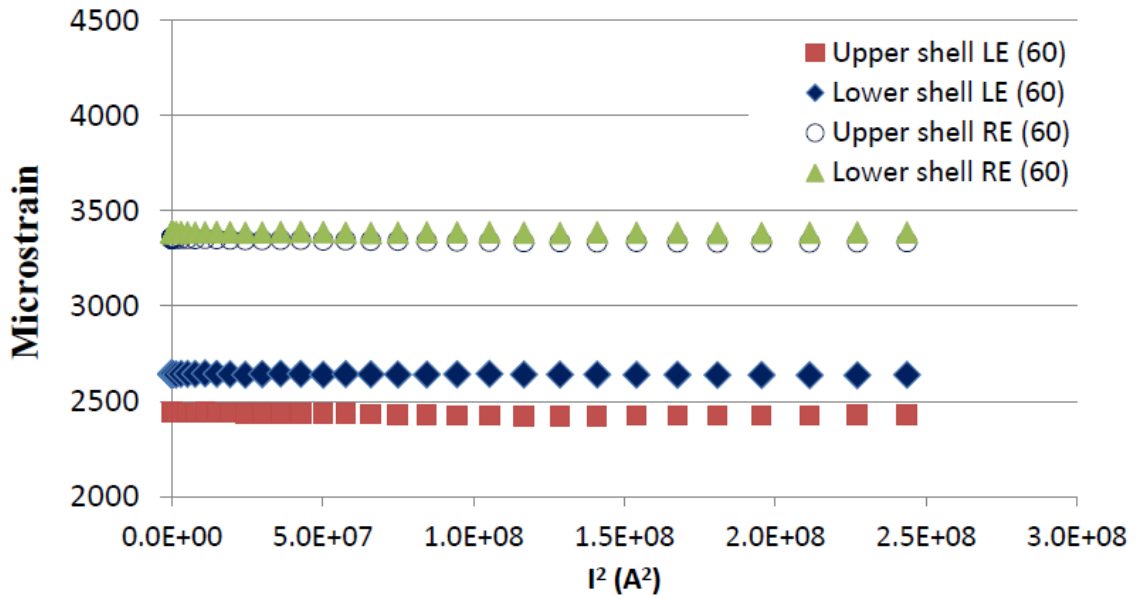


Fig. 28: Skin azimuthal microstrain at 60° vs. I^2 (A²) for quench 46 (14.6 kA).

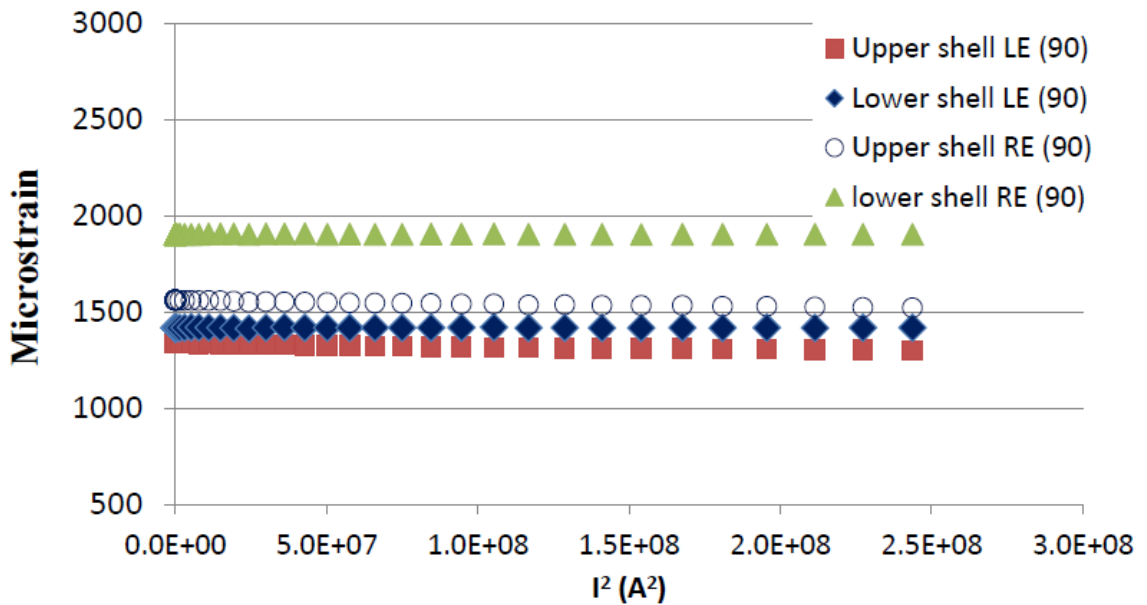


Fig. 29: Skin azimuthal microstrain at 90° vs. I^2 (A²) for quench 46 (14.6 kA).

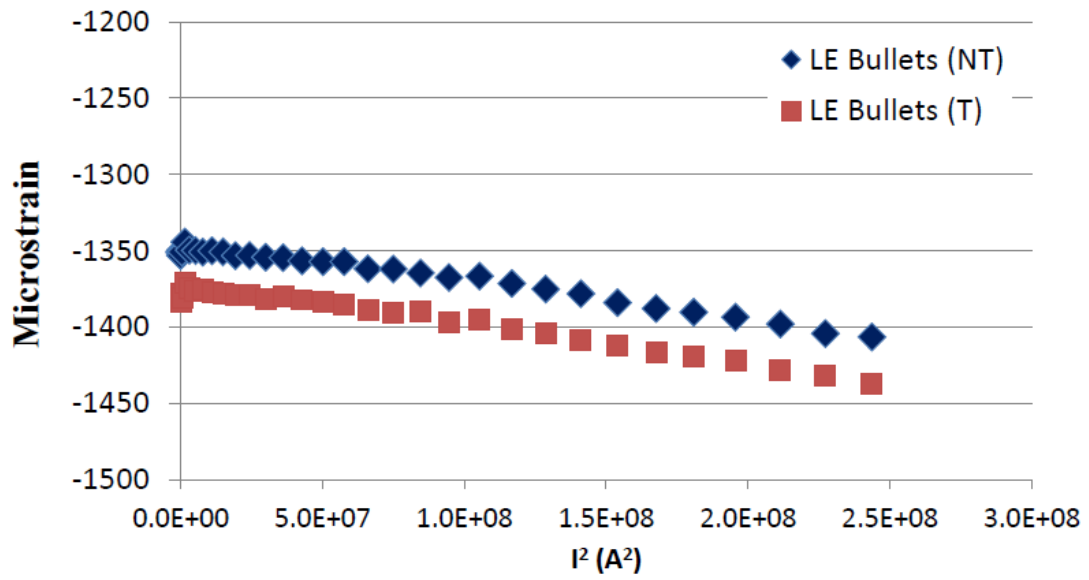


Fig. 30: Axial microstrain in the LE bullets vs. $I^2 \text{ (A}^2\text{)}$ for quench 46 (14.6 kA).

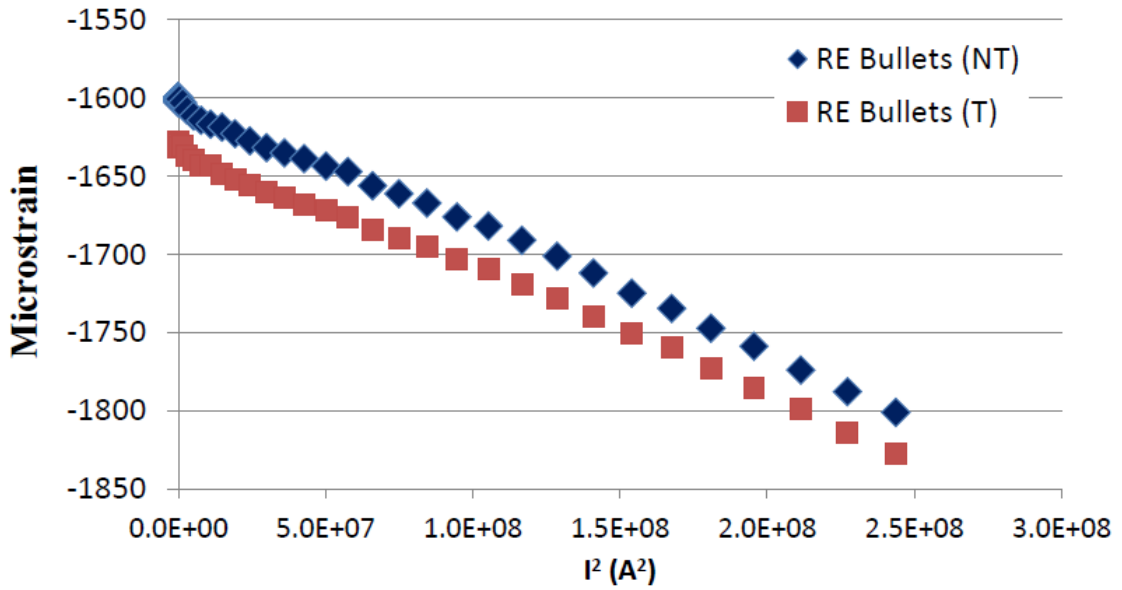


Fig. 31: Axial microstrain in the RE bullets vs. $I^2 \text{ (A}^2\text{)}$ for quench 46 (14.6 kA).

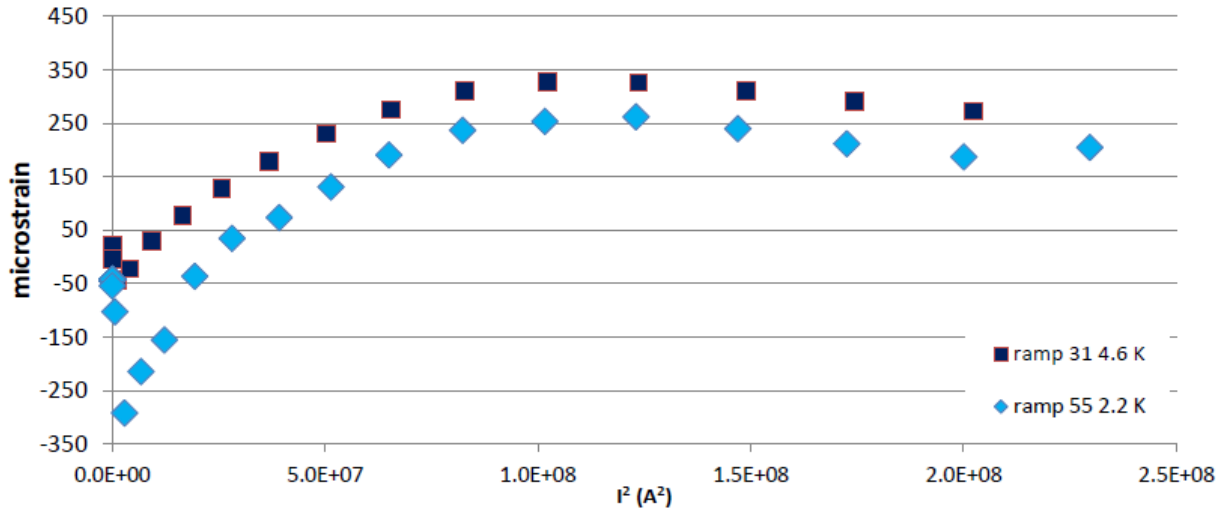


Fig. 32: Azimuthal microstrain in the coil pole vs. I^2 (A²) at 4.6 K and 2.2 K.

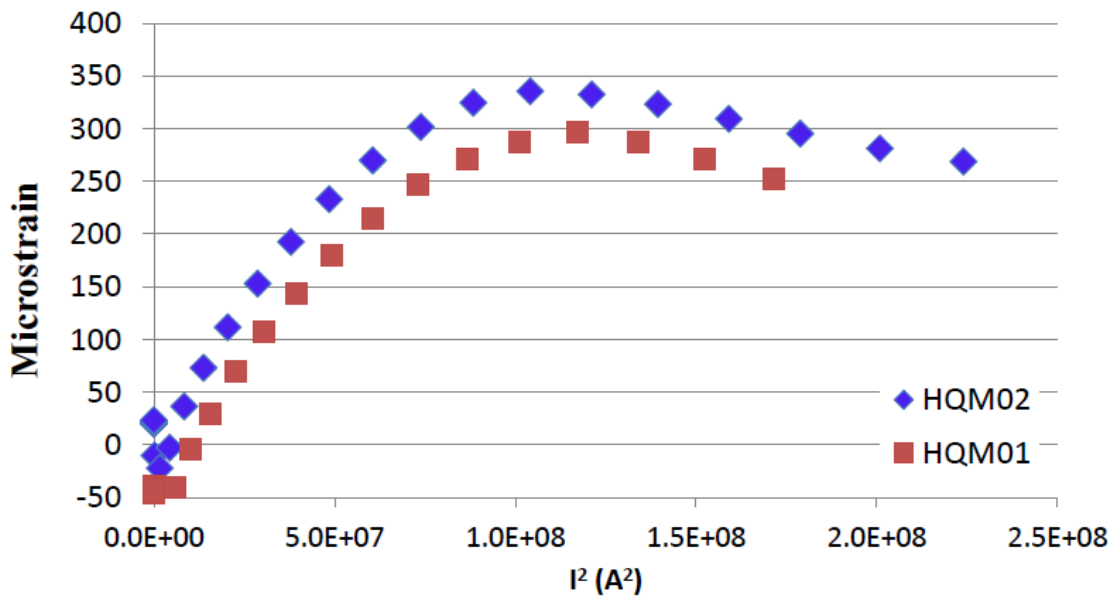


Fig. 33: Azimuthal microstrain in the coil pole vs. I^2 (A²) for HQM01 and HQM02 at 4.6 K.

7.3 Warm-up

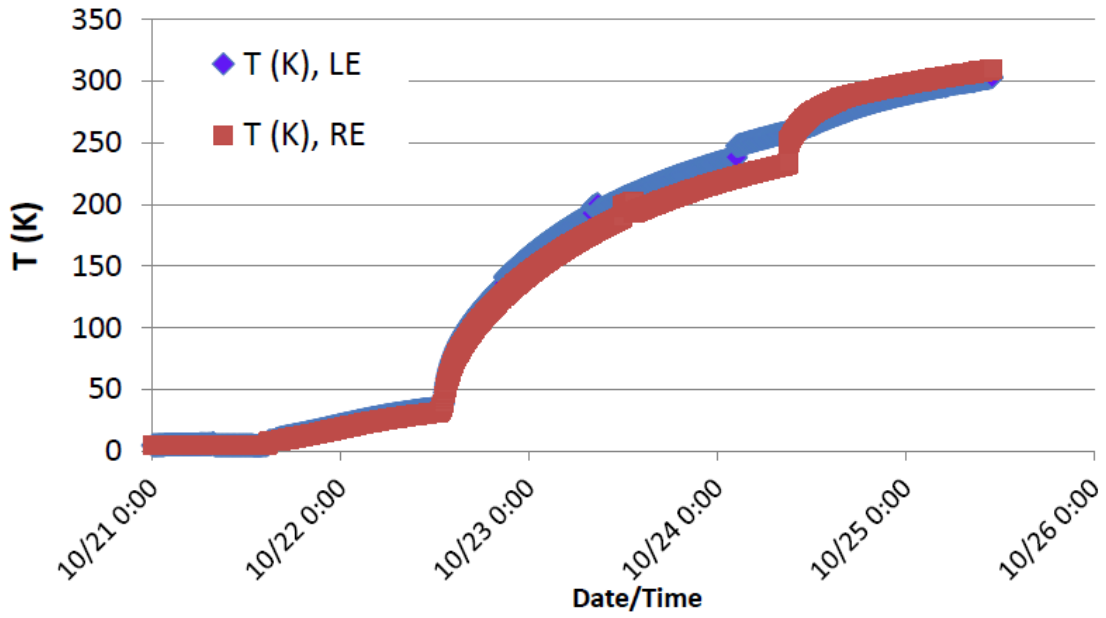


Fig. 34: Temperature of the magnet skin at LE and RE measured during warm-up vs. time.

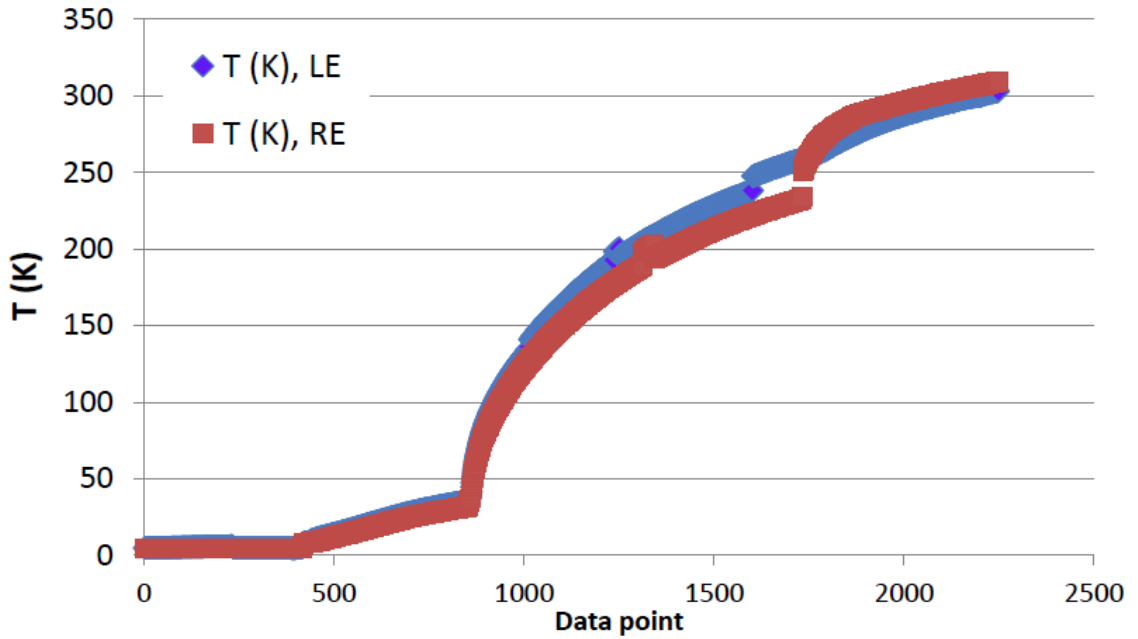


Fig. 35: Temperature of the magnet skin at LE and RE measured during warm-up vs. data point.

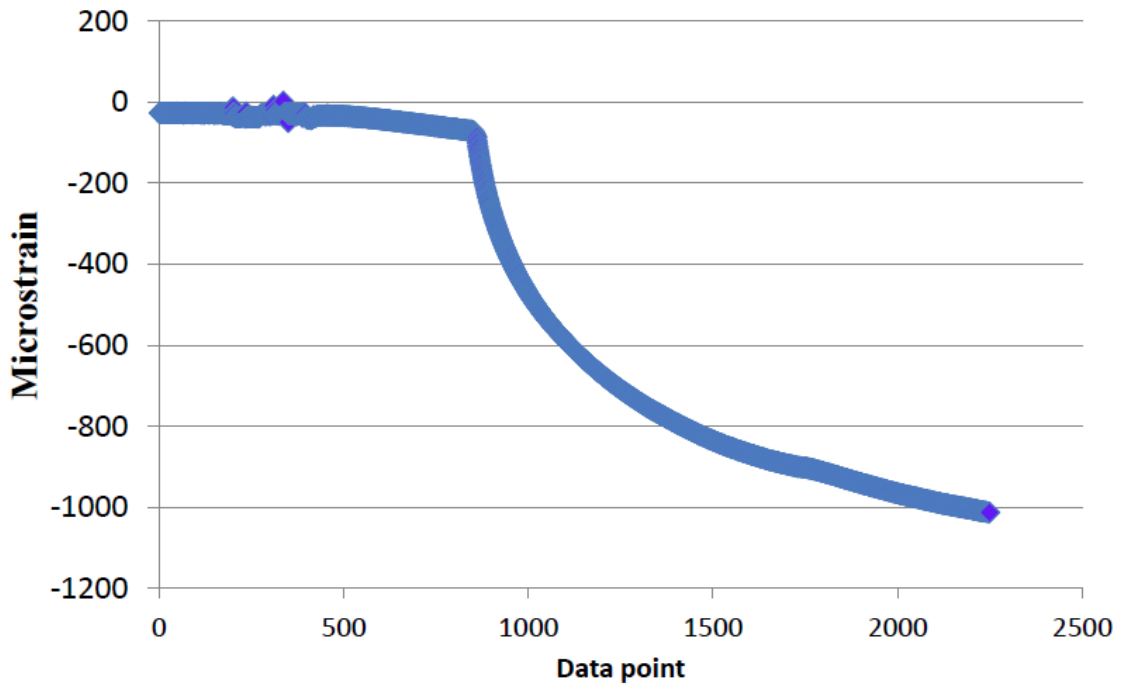


Fig. 36: Azimuthal microstrain in the coil pole measured during warm-up.

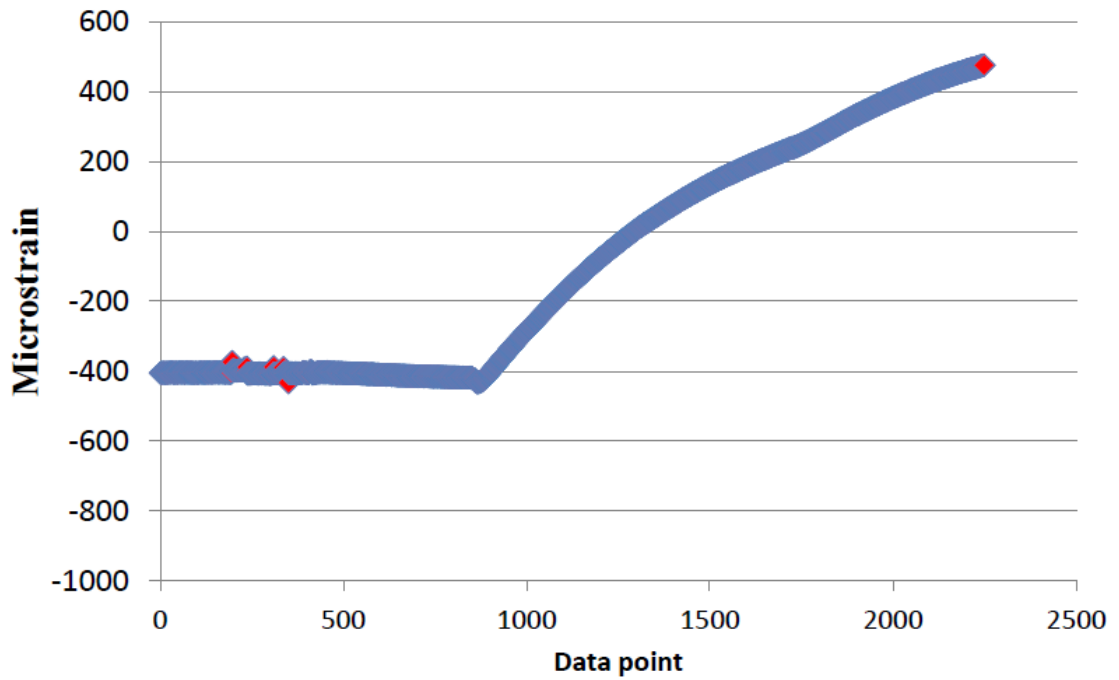


Fig. 37: Axial microstrain in the coil pole measured during warm-up.

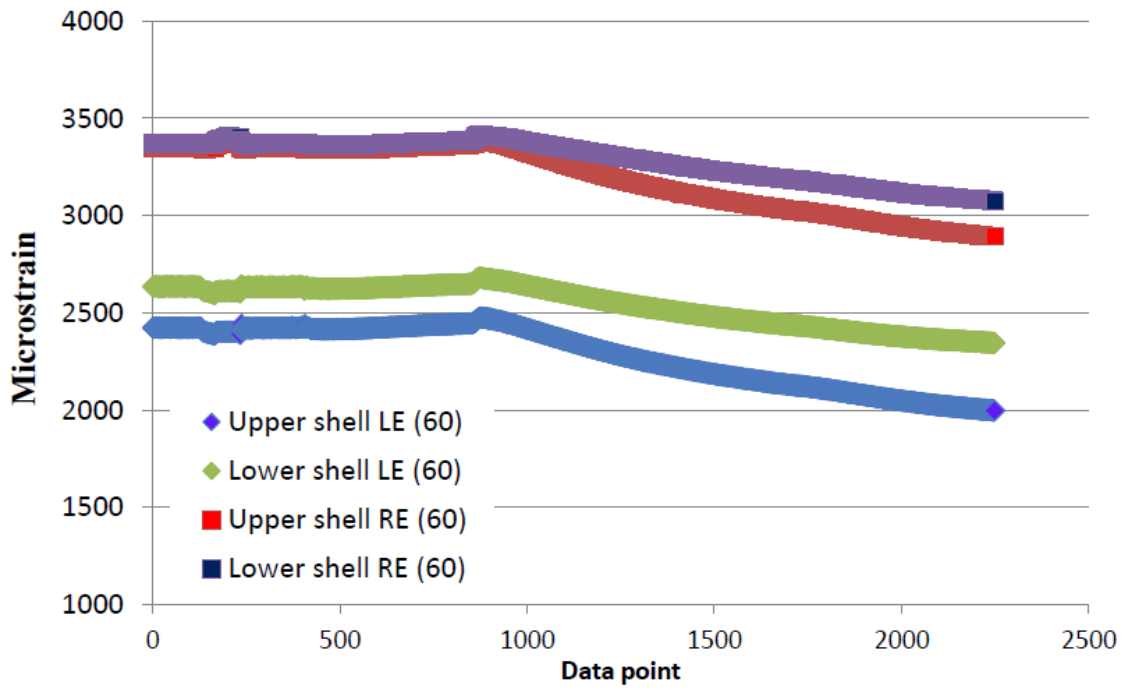


Fig. 38: Skin gauges at 60° during warm-up.

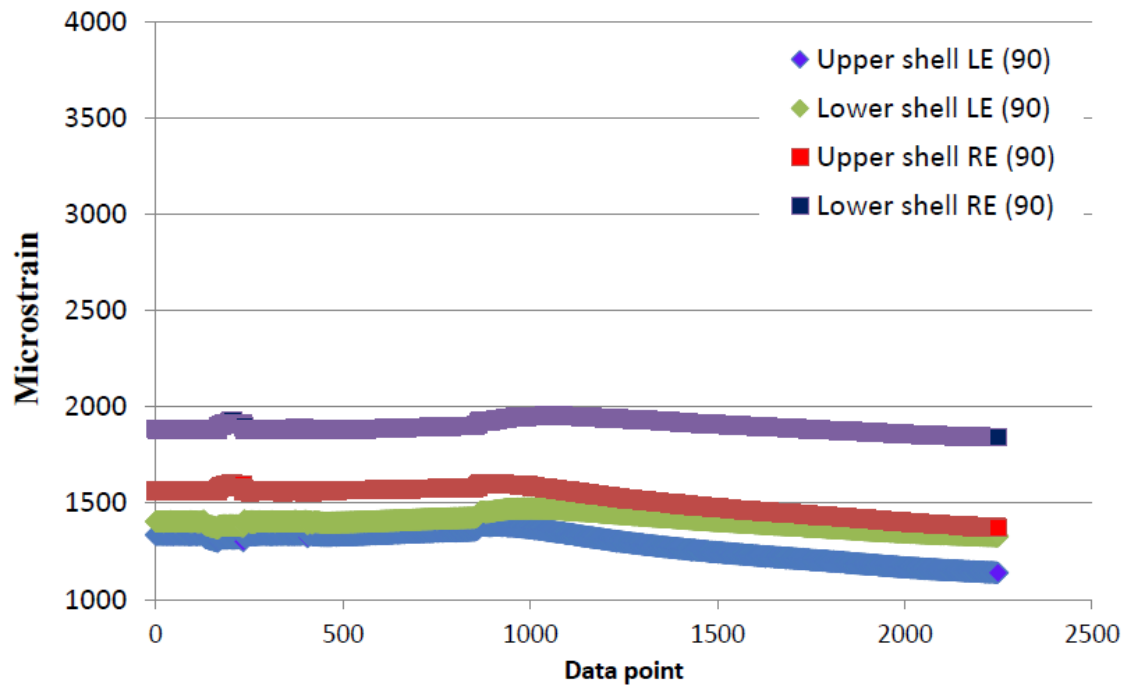


Fig. 39: Skin gauges at 90° during warm-up.

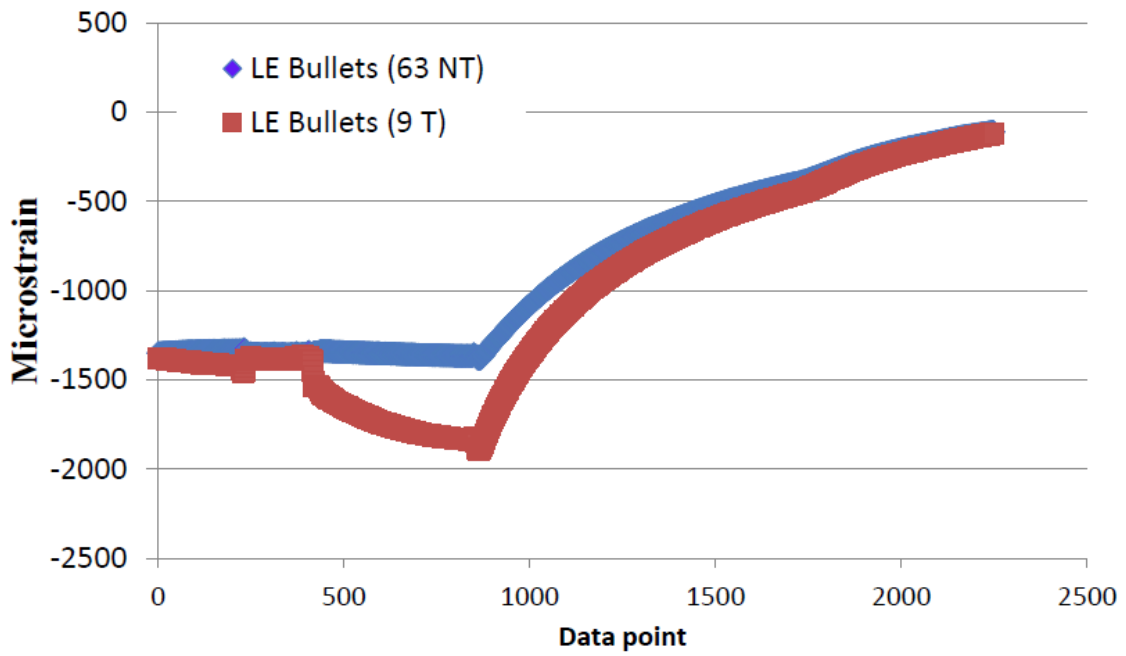


Fig. 40: LE bullet gauges during warm-up.

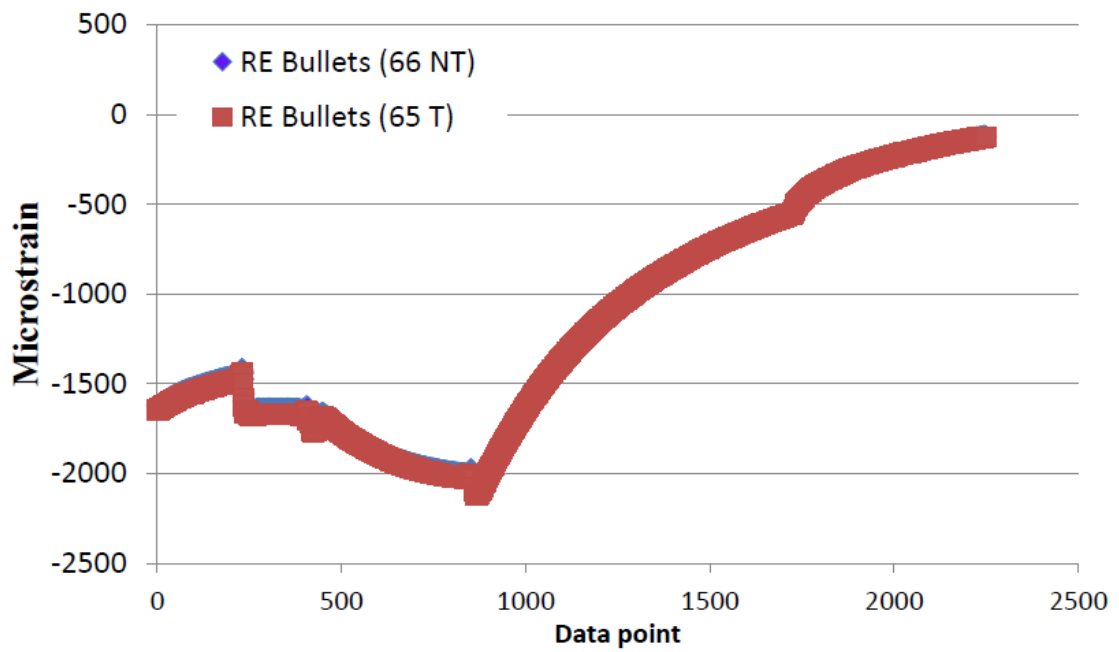


Fig. 41: RE bullet gauges during warm-up.

8. Protection Heater Study

Coil 13 was equipped with 25- μm -thick stainless steel protection heaters. 2 heaters were placed both on the inner and outer coil surfaces, one on the transition side (inner to outer coil layer transition) and one on the non-transition side.

Protection heater (PH) studies were done at 4.6 K and only with the inner layer heaters due to the electrical short between both outer layer heaters and the coil. The inner layer non-transition PH was fired, while the inner layer transition heater was protecting the magnet. Quench delay (time delay from the heater-firing-time to the quench-onset-time) as a function of the magnet current is shown in Fig. 42.

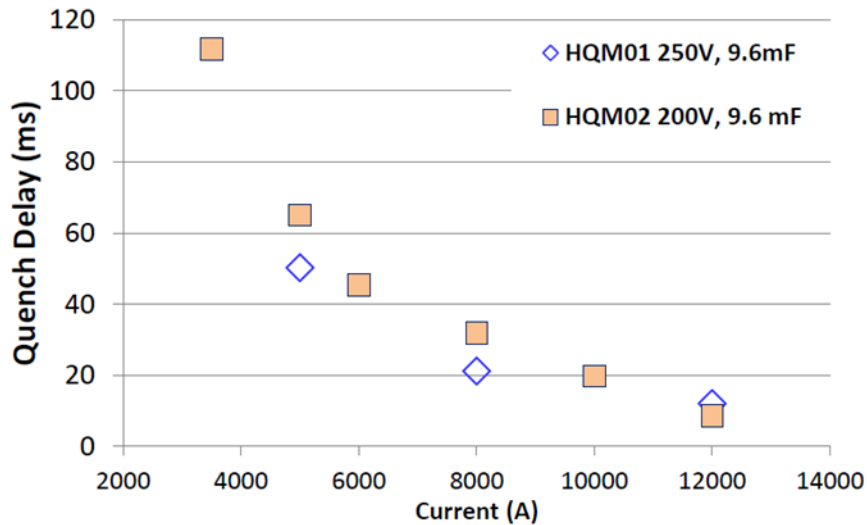


Fig. 42: Quench delay as a function of magnet current for HQM02 (HQM01 also shown for comparison). HFU capacitance and voltage are given.

9. Spike Data Analysis

A voltage spike detection system (VSDS) based on a National Instruments PXI multifunction DAQ was used to study thermo-magnetic instabilities in the HQM02 magnet. The VSDS captures half-coil signals at a sampling rate of 100 kHz. More details on this system are presented in [7]-[8]. VSDS data were used to adjust quench detection thresholds.

The number of voltage spikes as a function of magnet current at 4.6 K is shown in Fig. 43. The largest amount of spikes is detected around 1 kA.

Maximum spike voltage as a function of magnet current both at 4.6 K and 2.2 K is shown in Fig. 44. Almost all current spikes at 4.6 K are larger than at 2.2 K. A two-peak structure in the spike distributions is caused by different ramp rates used during quench training.

Spikes in HQM01 and HQM02 at 4.6 K are compared in Fig. 45. For magnet currents above 3 kA spikes in HQM01 are larger than in HQM02. As mentioned in Section 3, for

quench training we were ramping at 150-200 A/s up to 4 kA and then at lower ramp rates until a quench occurred. Therefore we can conclude that voltage spikes in HQM01 were larger than in HQM02 for ramp rates of 100 A/s and less. Larger spikes in HQM01 could be an indication for damage and increased instability in coil 12.

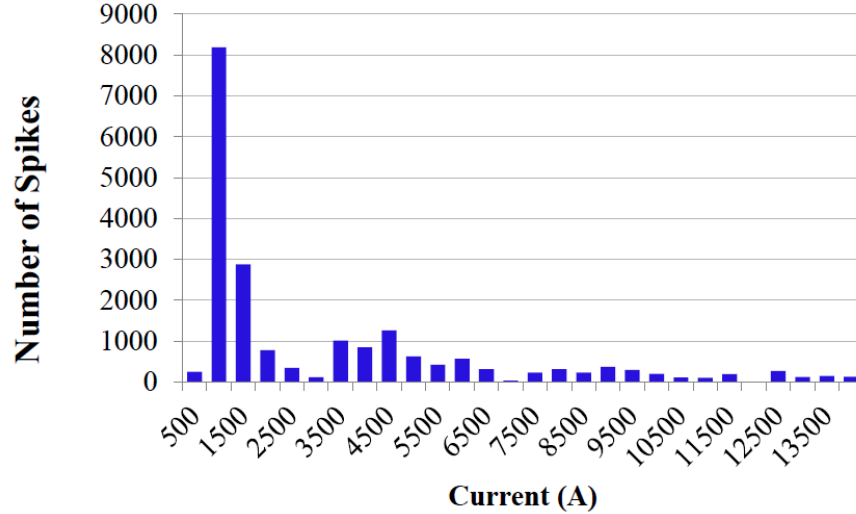


Fig. 43: Number of voltage spikes as a function of magnet current at 4.6 K.

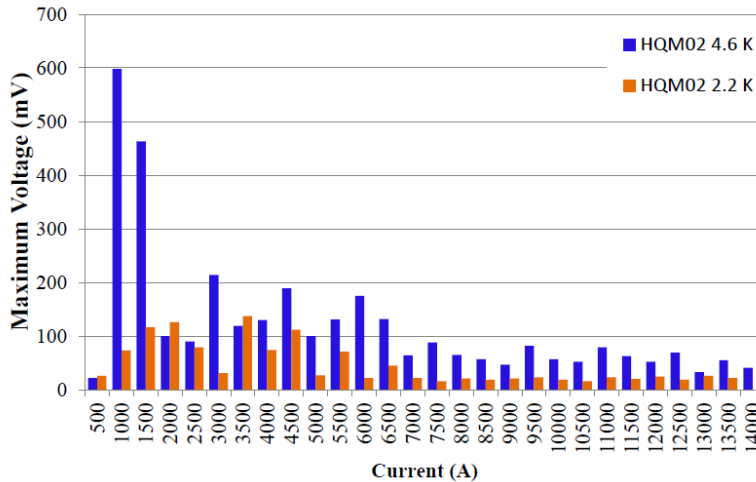


Fig. 44: Maximum voltage spike values as a function of magnet current.

10. Protection heater failure

The third training quench at 4.6 K resulted in an electrical short between the outer layer protection heaters and the magnet coil. This short most likely developed during the quench, since the active ground fault system did not trip before the quench and slow ramp down of the magnet current was not initiated. The HFU discharge profile and ground

fault current also confirm that the heater failure occurred only after the quench was detected ($t > 0$ in Fig. 46), when highest current and field were achieved.

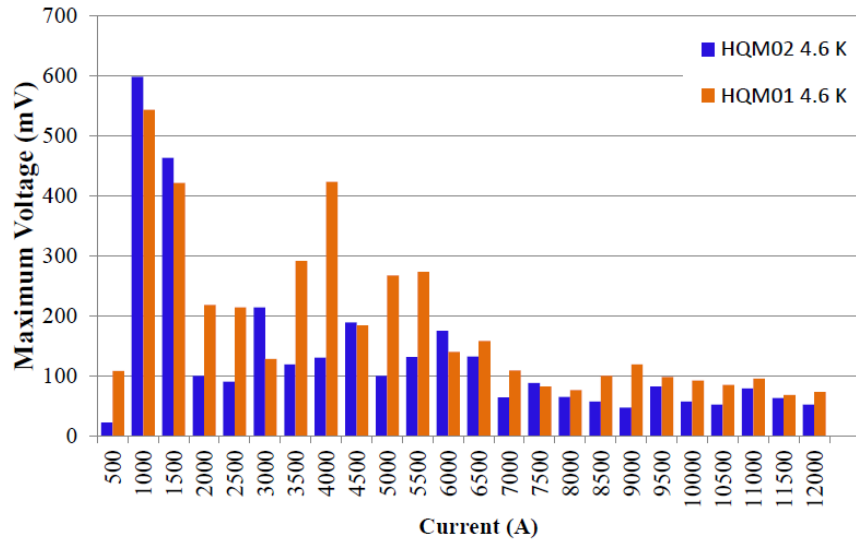


Fig. 45: Maximum voltage spike values as a function of magnet current in HQM01 and HQM02 at 4.6 K.

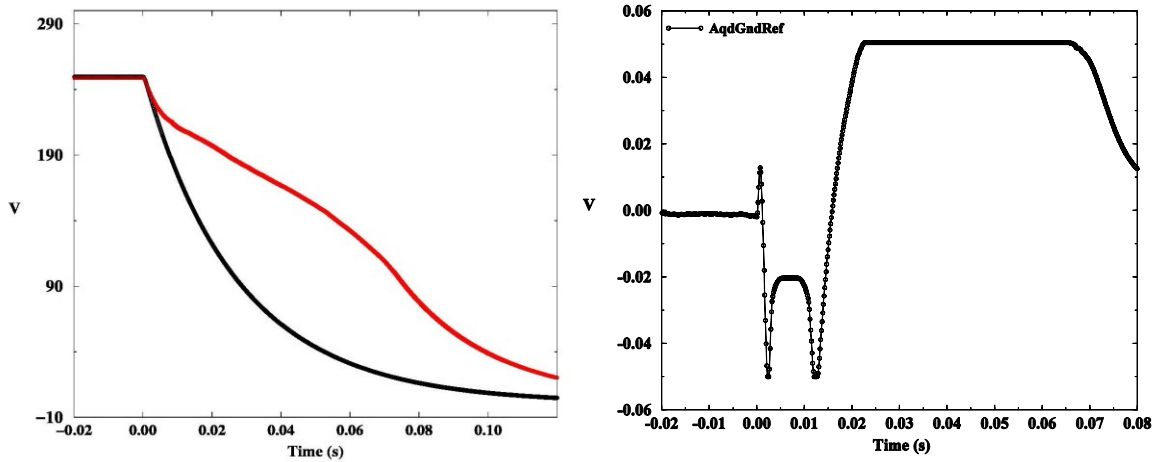


Fig. 46: HFU discharge for the inner (black) and outer (red) layer heaters (left) and ground fault current (right) in training quench #3

Testing was interrupted in order to investigate possible consequences for test safety. The main concern was if the ground insulation was compromised after the above mentioned failure.

Multiple manual trips were initiated to investigate signal noise levels. Afterwards, heater provoked quenches were initiated, gradually increasing the quench current. In these tests one of the inner layer heaters was protecting the magnet, while the other one

was fired. Noise level and strain gauge data did not exhibit any suspicious behavior, which could be indicating damaged ground insulation.

After the test we found the outer layer heaters burned at the return end of the stainless steel spacer (Fig. 47). Post-test electrical checkout showed that both outer layer heaters were shorted to the spacer and to the coil at the same time. No short was found between the coil and the return end splice block (metal part after the last current block).



Fig. 47: HQ coil 13 after the test

The heater failure is still under investigation. It is not understood yet if the coil-to-spacer short developed after quench #3 or if it was already present before the test.

Pre-load levels at the coil ends in the mirror structure are much less than in HQ quadrupoles with a shell-based structure (tens of kN vs. hundreds of kN). Therefore, large Lorentz forces could cause damage of the heater trace or insulation between the heater trace and the metal parts. In all cases enhanced insulation under the heater traces will help to prevent such a failure in the future.

11. Summary

Succeeding HQM01, a second HQ quadrupole coil with a 120-mm bore has been tested in a mirror structure (HQM02). Under the same pre-stress conditions, HQM02 exhibited much improved quench performance, and showed the best performance among all HQ coils tested so far. A SSL of 91% at 4.6 K and 89% at 2.2 K was achieved.

REFERENCES

1. S.A. Gourlay *et al.*, “Magnet R&D for the LHC Accelerator Research Program”, *IEEE Trans. Appl. Supercond.*, vol. 16, no.2, pp. 324-327, June 2006.
2. P. Wanderer *et al.*, “Overview of LARP Magnet R&D”, *IEEE Trans. Appl. Supercond.*, vol. 19, no.3, pp. 1208-1211, June 2009.
3. S. Hong *et al.*, “Latest improvements of current carrying capability of niobium tin and its magnet applications”, *IEEE Trans. on Applied Superconductivity*, vol. 16, Issue 2, 2005, p. 1146.
4. M.J. Lamm, *et al.*, “A New Facility to Test Superconducting Accelerator Magnets” *Proceedings of PAC97*, pp. 3395-3397
5. G. Chlachidze, *et al.*, “The Study of Single Nb₃Sn Quadrupole Coils Using a Magnetic Mirror Structure”, *IEEE Transactions on Applied Supercond.*, vol. 21, no. 3, pp. 1692-1695, June 2011.
6. <http://cp.literature.agilent.com/litweb/pdf/5965-4971E.pdf>
7. B. Bordini *et al.*, “Voltage spikes in Nb₃Sn and NbTi Strands”, *IEEE Trans. Appl. Superconduct.*, Vol. 16, Issue 2, June 2006, pp. 366-369
8. D.F. Orris *et al.*, “Voltage Spike Detection in High Field Superconducting Accelerator Magnets,” *IEEE trans. Appl. Superconduct.*, Vol. 15, Issue 2, June 2005, pp. 1205-1208

Appendix I

Table 1: HQM02 Quench History with comments

File	Qnch #	Current (A)	dI/dt (A/sec)	t _{quench} (sec)	MITs (10 ⁶ A ² sec)	QDC	Ave. Mag Temp (K)	Comments (online/offline)
hqm02.Quench.110912170328.917	-	1000	0	0.0007	0.17	HcoilHcoil	4.598	Trip at 1000 A after AQD balancing
hqm02.Quench.110912172248.309	-	3500	0	-0.6092	8.57	WcoilIdot	4.591	HFU2 testing 250V, 9.6mF, HFU1 in prot., 4.6 K
hqm02.Quench.110912180258.520	-	12110	20	0.0013	6.93	SIWcoil	4.593	DQD leads (Culeads) trip at 12kA, 20 A/s (150 A/s up to 4kA, 50 A/s up to 6.5kA) 4.6K
hqm02.Quench.110912185814.864	1	13608	20	-0.0136	10.67	HcoilHcoil	4.600	quench at 13.6 kA, 20 A/s, 4.6K
hqm02.Quench.110913113418.687	-	11972	20	0.0011	6.91	SIWcoil	4.567	AQD leads trip at 12 kA, 20 A/s, 4.6K
hqm02.Quench.110913120410.259	2	14034	20	-0.0146	11.35	HcoilHcoil	4.620	20 A/s, 4.6 K, after AQD CuLeads balanced at 9 kA
hqm02.Quench.110913124532.913	3	15719	20	-0.0094	11.45	HcoilHcoil	4.629	DQD leads trip at 15.7 kA, 20 A/s, 4.6K
hqm02.Quench.110915150514.585	-	1000	50	0.0008	0.17	GndRef	4.605	manual trip at 1000A, 50A/s, 4.6K
hqm02.Quench.110915164644.951	-	3500	150	-0.4444	6.57	WcoilIdot	4.606	HFU2 testing at 3.5 kA, both HFUs at 200V, 9.6 mF
hqm02.Quench.110915173813.724	-	5000	50	-0.1532	5.87	WcoilIdot	4.605	HFU2 testing at 5 kA, both HFUs at 200V, 9.6mF
hqm02.Quench.110920154534.355	-	6000	50	-0.0753	5.34	WcoilIdot	4.585	HFU2 testing at 6 kA, both HFUs at 200V, 9.6mF
hqm02.Quench.110920164523.997	-	8000	50	-0.0385	6.53	WcoilIdot	4.597	HFU2 testing at 8000A, 200V, 9.6mF, 4.6 K
hqm02.Quench.110920171016.354	-	10000	50	-0.0255	8.13	WcoilIdot	4.587	HFU2 test at 10 kA, 200V, 9.6mF, 4.6K
hqm02.Quench.110920175216.233	-	12000	50	-0.0151	9.33	WcoilIdot	4.611	HFU2 testing at 12 kA, 200V,9.6mF, 4.6K
hqm02.Quench.110921094602.388	-	13592	20	0.001	8.00	SIWcoil	4.604	DQD CuLeads trip at 13.5 kA, 20 A/s, 4.6K
hqm02.Quench.110921101600.723	-	14000	50	-0.0105	10.52	HcoilHcoil	4.619	HFU2 testing at 14 kA, 200V, 9.6mF, 4.6K
hqm02.Quench.110921120801.224	4	15881	20	-0.0133	12.65	HcoilHcoil	4.596	quench at 15.8 kA, 20 A/s, 4.6K
hqm02.Quench.110921143536.269	-	15419	20	0.0008	9.02	SIWcoil	4.599	DQD CuLeads trip at 15.3 kA, 20 A/s, 4.6K
hqm02.Quench.110921152024.806	5	16115	20	-0.0126	12.62	HcoilHcoil	4.601	quench at 16060A, 20 A/s, 4.6K
hqm02.Quench.110921160233.999	6	16367	20	-0.0052	11.17	HcoilHcoil	4.601	quench at 16340 A, 20 A/s, 4.6K
hqm02.Quench.110921164102.497	7	16390	20	-0.0034	10.72	HcoilHcoil	4.605	quench at 16.4 kA, 20 A/s, 4.6 K
hqm02.Quench.110921171636.595	8	16574	20	-0.0098	12.30	HcoilHcoil	4.606	quench at 16.5 kA, 20 A/s, 4.6K
hqm02.Quench.110921175730.806	9	16600	20	-0.0112	12.63	HcoilHcoil	4.608	quench at 16.5kA, 20A/s, 4.6K

hqm02.Quench.110922093609.571	10	16696	20	-0.0179	14.61	WcoilIdot	4.623	quench at 16.7 kA, 20 A/s, 4.6K
hqm02.Quench.110922103134.112	11	16699	20	-0.0083	11.91	WcoilIdot	4.618	quench at 16.7 kA, 20 A/s, 4.6K
hqm02.Quench.110922143443.155	12	16629	20	-0.0042	11.00	HcoilHcoil	4.604	quench at 16.6 kA, 20 A/s, 4.6K
hqm02.Quench.110922152132.562	13	16721	20	-0.0069	11.52	WcoilIdot	4.606	quench at 16.7 kA, 20 A/s, 4.6K
hqm02.Quench.110922160645.142	14	16718	20	-0.0076	11.73	SIWcoil	4.606	quench at 16.7 kA, 20 A/s, 4.6K
hqm02.Quench.110922165619.844	15	16858	5	-0.0067	11.60	WcoilIdot	4.612	quench at 16.8 kA, 5 A/s, 4.6K
hqm02.Quench.110922174549.436	16	16547	50	-0.0077	11.60	WcoilIdot	4.603	quench at 16.5 kA, 50 A/s, 4.6 K
hqm02.Quench.110922181834.901	17	16247	100	-0.0092	11.79	HcoilHcoil	4.608	quench at 16.2 kA, 100 A/s, 4.6 K
hqm02.Quench.110922185300.842	18	15940	150	-0.0099	11.71	HcoilHcoil	4.599	quench at 15.9 kA, 150 A/s, 4.6K
hqm02.Quench.110923084711.497	19	15548	200	-0.0059	10.72	HcoilHcoil	4.621	quench at 15.5 kA, 200 A/s, 4.6 K
hqm02.Quench.110923092936.558	20	15163	250	-0.0064	10.51	HcoilHcoil	4.610	quench at 15 kA, 250 A/s, 4.6 K
hqm02.Quench.110923102209.036	21	14757	300	-0.0062	10.13	HcoilHcoil	4.607	quench at 14757A, 300 A/s, 4.6 K
hqm02.Quench.110923104139.042	22	4747	400	-0.2184	6.85	HcoilHcoil	4.616	quench at 4.9 kA, 400 A/s, 4.6 K
hqm02.Quench.110923110225.739	23	14411	350	-0.0066	9.89	HcoilHcoil	4.610	quench at 14.4 kA, 350 A/s, 4.6K
hqm02.Quench.110927155202.207	24	14225	375	-0.0063	9.70	HcoilHcoil	4.616	quench at 14.2 kA, 375 A/s, 4.6 K
hqm02.Quench.110927162612.895	25	4755	400	-0.2118	6.71	HcoilHcoil	4.632	quench at 4.8 kA, 400 A/s, 4.6 K
hqm02.Quench.110927164720.632	26	3769	450	-0.3789	6.93	HcoilHcoil	4.627	quench at 3.9 kA, 450 A/s, 4.6 K
hqm02.Quench.110928111400.907	27	16969	20	-0.0139	13.97	HcoilHcoil	2.161	quench at 17 kA, 20 A/s, 2.2 K
hqm02.Quench.110928115257.838	28	17400	20	-0.0119	13.73	HcoilHcoil	2.147	quench at 17.4 kA, 20 A/s, 2.2K
hqm02.Quench.110928122857.653	29	17537	20	-0.0094	13.06	HcoilHcoil	2.156	quench at 17.5 kA, 20 A/s, 2.2 K
hqm02.Quench.110928140120.832	30	17751	20	-0.0063	12.55	HcoilHcoil	2.157	quench at 17.7 kA, 20 A/s, 2.2K
hqm02.Quench.110928151708.138	31	17831	20	-0.0115	13.99	WcoilGnd	2.166	quench at 17.8 kA, 20 A/s, 2.2 K
hqm02.Quench.110928160126.930	32	17779	20	-0.0036	11.85	HcoilHcoil	2.156	quench at 17.8 kA, 20 A/s, 2.2 K
hqm02.Quench.110928164957.892	33	17914	20	-0.007	12.57	SIWcoil	2.161	quench at 17.9 kA, 20 A/s, 2.2 K
hqm02.Quench.110929092855.539	34	18119	20	-0.0066	12.57	HcoilHcoil	2.148	quench at 18.1 kA, 20 A/s, 2.2 K
hqm02.Quench.110929101512.641	35	17980	20	-0.0067	12.70	HcoilHcoil	2.153	quench at 18 kA, 20 A/s, 2.2 K
hqm02.Quench.110929104808.997	36	18182	20	-0.0069	12.71	HcoilHcoil	2.152	quench at 18.2 kA, 20 A/s, 2.2 K
hqm02.Quench.110929130538.845	37	17905	20	-0.0064	12.40	SIWcoil	2.147	quench at 17.9 kA, 20 A/s, 2.2 K
hqm02.Quench.110929142722.392	38	18091	20	-0.0087	13.10	HcoilHcoil	2.156	quench at 18 kA, 20 A/s, 2.2K
hqm02.Quench.110929155158.029	39	18166	5	-0.0091	13.46	HcoilHcoil	2.155	quench at 18.2 kA, 5 A/s, 2.2 K

hqm02.Quench.110929163015.588	40	17573	100	-0.0095	13.06	HcoilHcoil	2.154	quench at 17.6 kA, 100 A/s, 2.2 K
hqm02.Quench.110929165846.605	41	18062	50	-0.0073	12.79	HcoilHcoil	2.146	quench at 18kA, 50 A/s, 2.2 K
hqm02.Quench.111006115902.230	42	18245	5	-0.002	11.48	HcoilHcoil	2.165	quench at 18.2 kA, 5 A/s, 2.2 K
hqm02.Quench.111006121857.533	43	16448	200	-0.0036	10.76	HcoilHcoil	2.164	quench at 16.5 kA, 200 A/s, 2.2 K
hqm02.Quench.111006125313.413	44	15495	300	-0.0052	10.45	HcoilHcoil	2.164	quench at 15.5 kA, 300 A/s, 2.2 K
hqm02.Quench.111006133226.549	45	15012	350	-0.0043	9.85	HcoilHcoil	2.162	quench at 15 kA, 350 A/s, 2.2 K
hqm02.Quench.111010110526.621	46	15194.1	375	-0.0094	11.2	WcoilIdot	2.151	quench at 15.2 kA, 375 A/s, 2.2 K
hqm02.Quench.111010112525.229	47	14888	375	-0.0057	10.06	HcoilHcoil	2.158	quench at 14.9 kA, 375 A/s, 2.2 K
hqm02.Quench.111010115801.654	48	14623	400	-0.0169	12.24	HcoilHcoil	2.156	quench at 14.6 kA, 400A/s, 2.2K
hqm02.Quench.111010121858.665	49	3901	450	-0.3386	6.73	WcoilIdot	2.165	quench at 4 kA, 450 A/s, 2.2 K
hqm02.Quench.111010134825.410	50	18145	20	-0.0052	11.95	SIWcoil	2.183	quench at 18.1 kA, 20 A/s, 2.2K
hqm02.Quench.111010143330.528	51	17957	20	-0.0055	12.12	SIWcoil	2.615	quench at 17.9 kA, 20 A/s, 2.6K
hqm02.Quench.111010151430.342	52	17715	20	-0.0071	12.40	SIWcoil	3.101	quench at 17.7 kA, 20 A/s, 3.1K
hqm02.Quench.111010160659.852	53	17283	20	-0.0056	11.49	SIWcoil	3.797	quench at 17.3 kA, 20 A/s, 3.8K
hqm02.Quench.111010175454.526	54	16755	20	-0.0085	12.02	HcoilHcoil	4.543	quench at 16.7 kA, 20 A/s, 4.6 K
hqm02.Quench.111014113351.210	55	16688	20	-0.0074	11.67	WcoilIdot	4.622	quench at 16.7 kA, 20 A/s, 4.6 K
hqm02.Quench.111014120228.947	56	13923	400	-0.0063	9.44	HcoilHcoil	4.639	w pre-cycling up to 10 kA then to 0 A at 150 A/s
hqm02.Quench.111014123148.838	57	13515	450	-0.0073	9.26	HcoilHcoil	4.642	w pre-cycling up to 10 kA then to 0 A
hqm02.Quench.111014134510.914	58	3642	450	-0.4056	6.90	WcoilIdot	4.625	quench at 3.9 kA, 450 A/s, 4.6 K
hqm02.Quench.111014135604.588	-	15106	0	0.001	8.83	SIWcoil	4.632	Holding 15 kA for 1min (Trip in DQD Leads -CuL)
hqm02.Quench.111021105826.792	-	0	0	-0.0146	0.08	GndRef	4.574	CVT removed, one shorted to Gnd through 150 Ohm.
hqm02.Quench.111021112155.230	-	1000	0	0.0008	0.20	GndRef	4.575	CVT removed, one shorted to Gnd through 150 Ohm
hqm02.Quench.111021113653.867	-	0	0	0.0008	0.08	GndRef	4.568	CVT removed, leads shorted & gnd thr. 150 Ohm
hqm02.Quench.111021114829.645	-	1000	0	-0.0039	0.18	WcoilIdot	4.569	CVT removed, pos leads shorted & gnd thr. 150 Ohm
hqm02.Quench.111021121853.703	-	1000	0	-0.0022	0.18	WcoilIdot	4.562	CVT removed, pos leads shorted and connected to mag. leads (single pin) to check comm. mode noise

Table 2: HQM02 Quench History with parameters for the first two quenching segments

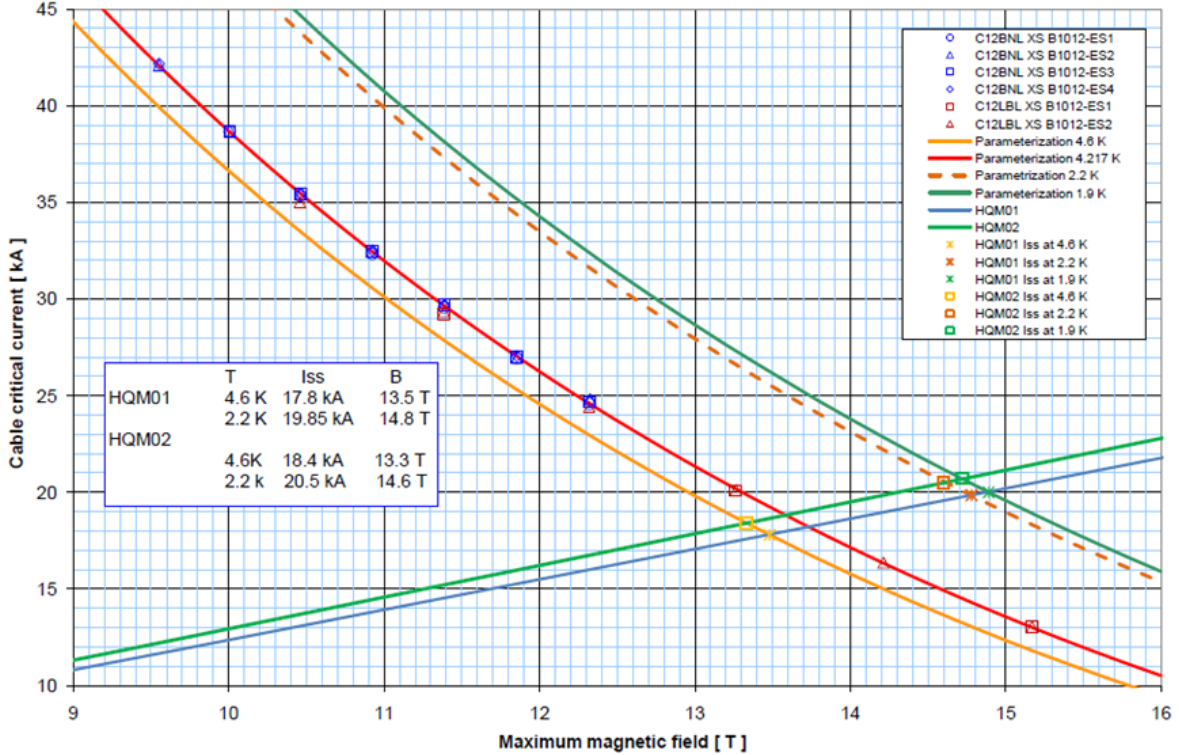
File	Qnch #	Current (A)	dI/dt (A/sec)	1st Vtap seg	trise (sec)	2nd Vtap seg	trise (sec)	Mag. Bot. Temp (K)	Mag. Top Temp (K)
hqm02.Quench.110912170328.917	-	1000	0	a7_a8	0.0003	a6_a7	0.0004	4.598	4.599
hqm02.Quench.110912172248.309	-	3500	0	b7_b6	-0.1540	b9_b8	-0.1323	4.595	4.587
hqm02.Quench.110912180258.520	-	12110	20	a3_a4	-0.0003	a9_a10	-0.0003	4.594	4.592
hqm02.Quench.110912185814.864	1	13608	20	b8_b7	-0.0199	b7_b6	-0.0160	4.602	4.597
hqm02.Quench.110913113418.687	-	11972	20	a9_a10	-0.0001	a8_a9	0.0006	4.566	4.568
hqm02.Quench.110913120410.259	2	14034	20	b8_b7	-0.0183	b9_b8	-0.0146	4.620	4.620
hqm02.Quench.110913124532.913	3	15719	20	a10_b10	-0.0095	a8_a9	-0.0069	4.631	4.628
hqm02.Quench.110915150514.585	-	1000	0					4.607	4.604
hqm02.Quench.110915164644.951	-	3500	0	a3_a4	-0.3400	a4_a5	-0.3400	4.608	4.605
hqm02.Quench.110915173813.724	-	5000	0	a4_a5	-0.1470	a3_a4	-0.1445	4.605	4.605
hqm02.Quench.110920154534.355	-	6000	0	a4_a5	-0.0731	a3_a4	-0.0693	4.585	4.584
hqm02.Quench.110920164523.997	-	8000	0	a4_a5	-0.0407	a3_a4	-0.0363	4.596	4.598
hqm02.Quench.110920171016.354	-	10000	0	a4_a5	-0.0186	a3_a4	-0.0183	4.591	4.584
hqm02.Quench.110920175216.233	-	12000	0	a6_a7	-0.0188	a7_a8	-0.0132	4.611	4.610
hqm02.Quench.110921094602.388	-	13592	20					4.605	4.603
hqm02.Quench.110921101600.723	-	14000	0	a6_a7	-0.0098	a4_a5	-0.0067	4.619	4.618
hqm02.Quench.110921120801.224	4	15881	20	a6_a7	-0.0141	a5_a6	-0.0126	4.598	4.594
hqm02.Quench.110921143536.269	-	15419	20					4.599	4.599
hqm02.Quench.110921152024.806	5	16115	20	a6_a7	-0.0134	b10_b9	-0.0116	4.603	4.600
hqm02.Quench.110921160233.999	6	16367	20	a6_a7	-0.0063	a5_a6	-0.0039	4.603	4.599
hqm02.Quench.110921164102.497	7	16390	20	a9_a10	-0.0046	a8_a9	-0.0024	4.607	4.602
hqm02.Quench.110921171636.595	8	16574	20	a6_a7	-0.0108	b10_b9	-0.0094	4.607	4.604
hqm02.Quench.110921175730.806	9	16600	20	a7_a8	-0.0119	b8_b7	-0.0105	4.609	4.606
hqm02.Quench.110922093609.571	10	16696	20	a10_b10	-0.0104	b10_b9	-0.0083	4.625	4.621
hqm02.Quench.110922103134.112	11	16699	20	a10_b10	-0.0105	b10_b9	-0.0090	4.620	4.617
hqm02.Quench.110922143443.155	12	16629	20	a6_a7	-0.0073	a5_a6	-0.0056	4.605	4.603

hqm02.Quench.110922152132.562	13	16721	20	a10_b10	-0.0106	b10_b9	-0.0084	4.606	4.606
hqm02.Quench.110922160645.142	14	16718	20	a10_b10	-0.0108	b10_b9	-0.0084	4.607	4.605
hqm02.Quench.110922165619.844	15	16858	5	a10_b10	-0.0099	b10_b9	-0.0084	4.613	4.610
hqm02.Quench.110922174549.436	16	16547	50	a10_b10	-0.0113	b10_b9	-0.0094	4.603	4.603
hqm02.Quench.110922181834.901	17	16247	100	a10_b10	-0.0116	b10_b9	-0.0092	4.606	4.609
hqm02.Quench.110922185300.842	18	15940	150	a10_b10	-0.0123	a8_a9	-0.0097	4.600	4.598
hqm02.Quench.110923084711.497	19	15548	200	b8_b7	-0.0060	b9_b8	-0.0036	4.621	4.621
hqm02.Quench.110923092936.558	20	15163	250	b8_b7	-0.0066	b7_b6	-0.0052	4.613	4.608
hqm02.Quench.110923102209.036	21	14757	300	b8_b7	-0.0064	b9_b8	-0.0036	4.607	4.607
hqm02.Quench.110923104139.042	22	4747	400	a3_a4	-0.0846	a2_a3	-0.0675	4.616	4.616
hqm02.Quench.110923110225.739	23	14411	350	b8_b7	-0.0066	b9_b8	-0.0035	4.610	4.610
hqm02.Quench.110927155202.207	24	14225	375	b8_b7	-0.0069	b5_b4	-0.0038	4.617	4.615
hqm02.Quench.110927162612.895	25	4755	400	a3_a4	-0.0849	a4_a5	-0.0748	4.631	4.633
hqm02.Quench.110927164720.632	26	3769	450	a10_b10	0.0008	a7_a8	0.0010	4.626	4.628
hqm02.Quench.110928111400.907	27	16969	20	a9_a10	-0.0144	a4_a5	-0.0109	2.162	2.160
hqm02.Quench.110928115257.838	28	17400	20	a7_a8	-0.0122	a4_a5	-0.0092	2.148	2.147
hqm02.Quench.110928122857.653	29	17537	20	a6_a7	-0.0102	b10_b9	-0.0092	2.157	2.155
hqm02.Quench.110928140120.832	30	17751	20	a7_a8	-0.0062	b9_b8	-0.0052	2.158	2.157
hqm02.Quench.110928151708.138	31	17831	20	a7_a8	-0.0101	b8_b7	-0.0085	2.170	2.162
hqm02.Quench.110928160126.930	32	17779	20	a10_b10	-0.0045	a4_a5	-0.0024	2.156	2.155
hqm02.Quench.110928164957.892	33	17914	20	a9_a10	-0.0097	b8_b7	-0.0080	2.163	2.158
hqm02.Quench.110929092855.539	34	18119	20	a7_a8	-0.0090	b8_b7	-0.0074	2.149	2.148
hqm02.Quench.110929101512.641	35	17980	20	a6_a7	-0.0077	a5_a6	-0.0071	2.154	2.152
hqm02.Quench.110929104808.997	36	18182	20	a7_a8	-0.0085	b8_b7	-0.0070	2.153	2.151
hqm02.Quench.110929130538.845	37	17905	20	a10_b10	-0.0099	a6_a7	-0.0078	2.149	2.146
hqm02.Quench.110929142722.392	38	18091	20	a7_a8	-0.0095	b8_b7	-0.0073	2.157	2.156
hqm02.Quench.110929155158.029	39	18166	5	a7_a8	-0.0097	b8_b7	-0.0085	2.157	2.154
hqm02.Quench.110929163015.588	40	17573	100	b8_b7	-0.0097	a7_a8	-0.0084	2.155	2.153
hqm02.Quench.110929165846.605	41	18062	50	a7_a8	-0.0080	b8_b7	-0.0066	2.145	2.148
hqm02.Quench.111006115902.230	42	18245	5	a10_b10	-0.0048	a8_a9	-0.0027	2.169	2.161

hqm02.Quench.111006121857.533	43	16448	200	b8_b7	-0.0045	b5_b4	-0.0042	2.168	2.161
hqm02.Quench.111006125313.413	44	15495	300	b8_b7	-0.0060	b5_b4	-0.0036	2.167	2.162
hqm02.Quench.111006133226.549	45	15012	350	b8_b7	-0.0056	b9_b8	-0.0029	2.162	2.161
hqm02.Quench.111010110526.621	46	15194.1	375	b8_b7	-0.007	b5_b4	-0.0041	2.1523	2.1498
hqm02.Quench.111010112525.229	47	14888	375	b8_b7	-0.0062	b5_b4	-0.0038	2.159	2.157
hqm02.Quench.111010115801.654	48	14623	400	b8_b7	-0.0060	b5_b4	-0.0035	2.158	2.154
hqm02.Quench.111010121858.665	49	3901	450	a7_a8	0.0008	a8_a9	0.0014	2.167	2.164
hqm02.Quench.111010134825.410	50	18145	20	a10_b10	-0.0087	a6_a7	-0.0069	2.178	2.188
hqm02.Quench.111010143330.528	51	17957	20	a10_b10	-0.0088	a6_a7	-0.0070	2.603	2.627
hqm02.Quench.111010151430.342	52	17715	20	a10_b10	-0.0098	a6_a7	-0.0078	3.101	3.102
hqm02.Quench.111010160659.852	53	17283	20	a10_b10	-0.0098	b10_b9	-0.0076	3.797	3.798
hqm02.Quench.111010175454.526	54	16755	20	a10_b10	-0.0102	b10_b9	-0.0085	4.546	4.541
hqm02.Quench.111014113351.210	55	16688	20	a10_b10	-0.0106	b10_b9	-0.0090	4.623	4.621
hqm02.Quench.111014120228.947	56	13923	400	b8_b7	-0.0080	b5_b4	-0.0049	4.640	4.638
hqm02.Quench.111014123148.838	57	13515	450	a3_a4	-0.0080	b4_b3	-0.0057	4.641	4.642
hqm02.Quench.111014134510.914	58	3642	450	a7_a8	0.0008	a8_a9	0.0014	4.628	4.622
hqm02.Quench.111014135604.588	-	15106	0					4.633	4.631
hqm02.Quench.111021105826.792	-	0	0					4.576	4.571
hqm02.Quench.111021112155.230	-	1000	0					4.575	4.575
hqm02.Quench.111021113653.867	-	0	0					4.569	4.568
hqm02.Quench.111021114829.645	-	1000	0					4.569	4.569
hqm02.Quench.111021121853.703	-	1000	0					4.563	4.561

Appendix II

HQM01 Coil 12 Short Sample estimate (06/14/2011 - H Felice - A. Ghosh - A Godeke - D. Dietderich)
 AVERAGE of the ES - Loadline provided by Vadim Kashikhin on 09/02/2011
 Extracted, self-field correction strand data: 0.457 T/kA



2011_09_06_HQM01_short-sample_average2.xlsm

9/6/2011

Short sample HQM